https://doi.org/10.5194/egusphere-2026-998
Preprint. Discussion started: 19 March 2026


# Enhancement of ammonium nitrate aerosol in the Northern Hemisphere lower stratosphere linked to Asian summer monsoon outflow

Fatih Ekinci[1,2*,5], Oliver Eppers[2*], Oliver Appel[1,2*], Felix Ploeger[3,10], Antonis Dragoneas[8], Sergej Molleker[7], Philipp Brauner[2*], Hans-Christoph Lachnitt[1], Franziska Weyland[1], Linda Ort[9], Nicolas Emig[1], Hans-Christian Clemen[2*], Laura Tomsche[1,4], Martin Ebert[5], Peter Hoor[1], Bärbel Vogel[3], Yafang Cheng[6], Johannes Schneider[2*], Stephan Borrmann[1,2], and Franziska Köllner[1,2*]

[1]Institute for Atmospheric Physics, University of Mainz, Mainz, Germany
[2]Particle Chemistry Department, Max Planck Institute for Chemistry, Mainz, Germany
[3]Institute of Climate and Energy Systems (ICE-4), Forschungszentrum Jülich, Jülich, Germany
[4]Institut für Physik der Atmosphäre, Deutsches Zentrum für Luft- und Raumfahrt (DLR), Oberpfaffenhofen, Germany
[5]Institute for Applied Geosciences (Environmental Mineralogy), Technical University of Darmstadt, Darmstadt, Germany
[6]Aerosol Chemistry Department, Max Planck Institute for Chemistry, Mainz, Germany
[7]Instrument Development Group, Max Planck Institute for Chemistry, Mainz, Germany
[8]Climate Geochemistry Department, Max Planck Institute for Chemistry, Mainz, Germany
[9]Atmospheric Chemistry Department, Max Planck Institute for Chemistry, Mainz, Germany
[10]Institute for Atmospheric and Environmental Research, University of Wuppertal, Wuppertal, Germany
[*]now at: Aerosol Chemistry Department, Max Planck Institute for Chemistry, Mainz, Germany

**Correspondence:** Franziska Köllner (f.koellner@mpic.de)

**Abstract.**

This study examines how Asian Summer Monsoon (ASM) outflow perturbs the chemical composition of background aerosol in the extratropical lower stratosphere (ExLS). We analyze the summer-to-autumn transition in aerosol chemical composition using in-situ measurements from the ERICA instrument acquired during the PHILEAS aircraft campaign in August-September 2023 over the North Pacific, Alaska, northern Canada, and northern Europe. We observe an enrichment of ammonium and nitrate aerosol in the ExLS background air masses from summer to autumn, particularly at potential temperatures above 370 K (~13 km). Concurrently, the fraction of $NO^+$-rich particles in the ExLS increases from August to September 2023. The corresponding mass spectra indicate internally mixed particles containing nitrate, sulfate, ammonium, and organic matter. Simulations with the Chemical Lagrangian Model of the Stratosphere (CLaMS) show this seasonal transition is associated with the intrusion of relatively young air masses (<3.5 months old) originating from South Asia and the western Pacific into the ExLS, especially in autumn. These particles persist in the lower stratosphere for weeks up to months and undergo chemical aging. This aging is reflected by an observed increasing oxidative degree of organic matter, a decreasing nitrate-to-sulfate ratio, and an increasing ammonium-to-nitrate ratio, suggesting progressive sulfate incorporation and particle nitrate depletion. Overall, our results demonstrate that the ASM outflow can substantially shape ExLS background aerosol composition through the convective uplift, subsequent transport, and aging of ammonium- and nitrate-rich air masses from polluted surface regions, with important implications for stratospheric heterogeneous chemistry and aerosol-climate interactions.

https://doi.org/10.5194/egusphere-2026-998
Preprint. Discussion started: 19 March 2026


## 1 Introduction

The Asian Summer Monsoon Anticyclone (AMA) is a major meteorological feature of the upper troposphere and lower stratosphere (UTLS) during the boreal summer. Driven by the convection of the Asian Summer Monsoon (ASM) over the Asian region, the AMA covers a large area from 20°E to 140°E, bounded latitudinally by the subtropical westerly jet to the north and the equatorial easterly jet to the south (Pan et al., 2016; Vogel et al., 2019; Gettelman et al., 2011; Annamalai and Slingo, 2001; Garny and Randel, 2013; Randel and Park, 2006). The AMA forms in June and persists through September. Centered over the Tibetan Plateau, it exhibits its strongest anticyclonic circulation close to the local tropopause around 17–18 km, which is the globally highest tropopause during the monsoon period (Brunamonti et al., 2018; Vogel et al., 2019; Vernier et al., 2011, 2018; Hanumanthu et al., 2020; Thomason and Vernier, 2013; Garny and Randel, 2016; Pan et al., 2016). Acting as a transport barrier (Ploeger et al., 2015), the AMA traps air masses enriched with trace gases and pollutants from ground-level sources, allowing their accumulation and vertical transport into the UTLS (e.g., Pan et al., 2016; Santee et al., 2017; Randel et al., 2010; Park et al., 2008). This makes the AMA in association with the ASM a major pathway for the redistribution of boundary layer emissions from Asia into the UTLS (Barth et al., 2001, 2007a, b; Vernier et al., 2011, 2018; Pan et al., 2016; Lawrence and Lelieveld, 2010; Müller et al., 2016; Vogel et al., 2016; Ploeger et al., 2017).

Along with the ASM season, the so-called Asian Tropopause Aerosol Layer (ATAL) forms every year in June and dissipates with the weakening of the ASM in September. The ATAL was first identified through CALIPSO satellite lidar measurements and later confirmed by in-situ balloon observations (Hanumanthu et al., 2020; Brunamonti et al., 2018; Vernier et al., 2015, 2018; Thomason and Vernier, 2013; Bian et al., 2020). This aerosol layer is characterized by an enrichment of aerosol particles between 13 and 18 km (Vernier et al., 2015; Mahnke et al., 2021), which are composed of solid ammonium nitrate (AN) particles as well as sulfates and organic matter (Höpfner et al., 2019; Yu et al., 2015; Appel et al., 2022; Vernier et al., 2022; Zhu et al., 2024; Yu et al., 2022; Xenofontos et al., 2024). The formation and persistence of the ATAL is driven by the rapid vertical uplift of precursor gases within the ASM and the secondary formation of new particles in the confinement of the AMA (Weigel et al., 2021; Mahnke et al., 2021; Appel et al., 2022; Höpfner et al., 2019; Xenofontos et al., 2024; Fairlie et al., 2020). Additionally, wet deposition plays an important role in shaping the aerosol composition within the UTLS. Recent observations show that primary aerosol species are removed with an efficiency exceeding 98% during convective transport in the ASM (Berberich et al., 2025). This extreme wet scavenging efficiency limits the direct transport of boundary layer aerosols into the UTLS, thereby reducing the condensation sink above the convection region. Consequently, nucleation processes in the ATAL are strongly favored, as the reduced competition for condensable vapors facilitates the formation of new particles. This highlights the critical interplay between wet deposition, reduced primary aerosol transport, and the subsequent enhancement of secondary aerosol formation in the ATAL as described in Appel et al. (2022). The ATAL has a significant impact on climate processes by cooling the atmosphere through direct short-term regional forcing (Vernier et al., 2015). Furthermore, it can influence the presence of ice clouds due to the ability of solid AN to form ice in cirrus conditions (Wagner et al., 2020). Observations show that the aerosol optical depth of the ATAL has increased significantly in recent decades, correlating with increasing emissions in Asia (Hanumanthu et al., 2020; Fadnavis et al., 2019; Yu et al., 2015). This highlights the ATAL's

https://doi.org/10.5194/egusphere-2026-998
Preprint. Discussion started: 19 March 2026


sensitivity to anthropogenic and natural sources (Vernier et al., 2015, 2018; Lawrence and Lelieveld, 2010; Thomason and Vernier, 2013; Pan et al., 2016).

The East-West oscillation of the AMA influences the eddy formation (Zhang et al., 2002a; Popovic and Plumb, 2001; Nützel et al., 2016) and atmospheric transport pathways (Vogel et al., 2014; Fadnavis et al., 2018). This also causes the redistribution of the polluted air masses through the AMA's eddy shedding dynamics (Hsu and Plumb, 1999; Popovic and Plumb, 2001; Honomichl and Pan, 2020; Vogel et al., 2016; Müller et al., 2016; Clemens et al., 2022, 2024). The so-called 'eddies' and the filaments from the AMA's eastern flank facilitate the mixing of confined tropospheric air masses into extratropical regions (Vogel et al., 2015; Gottschaldt et al., 2018; Fujiwara et al., 2021). Satellite data reveal that trace gases such as carbon monoxide (CO), peroxyacetyl nitrate (PAN), and nitrogen oxides ($NO_x$) are transported during eddy-shedding events primarily along two pathways: a western pathway toward Africa and the Mediterranean region, and an eastward pathway toward the western Pacific (Fadnavis et al., 2018). Lauther et al. (2022) have also used in-situ measurements of anthropogenic trace gases, such as dichloromethane, to demonstrate the transport by the AMA to the extratropical UTLS. Notably, eddy induced transport exhibits strong seasonal variability, with the most intense events occurring during peak monsoon activity (Fadnavis et al., 2018; Wang et al., 2022; Ungermann et al., 2016). Despite the progress in understanding the ATAL, significant knowledge gaps persist regarding the process of aerosols transported from the ASM region into the extratropical lower stratosphere (ExLS) (Khaykin et al., 2017; Graßl et al., 2024; Yu et al., 2017; Fadnavis et al., 2024). A recent analysis by Köllner et al. (2026) confirms the transport of AN particles and organic matter from Asia via the ASM convection and AMA filaments into the ExLS.

However, our knowledge about the residence time, the persistence, and the chemical processing of the aerosol from the ASM region when incorporated in the stratospheric background aerosol is incomplete. Filling these gaps is essential for assessing the broader impacts of AMA-driven transport on atmospheric chemistry and climate. For this reason, we investigated the chemical composition of aerosol particles in the extratropical UTLS region during boreal summer/autumn by the aircraft-based mission PHILEAS (Probing HIgh Latitude Export of air from the Asian Summer monsoon). The PHILEAS campaign, carried out with the HALO (High Altitude and LOng range) research aircraft, provides a unique opportunity to study these features (Riese et al., 2025). We used concurrent data from the aerosol mass spectrometer ERICA (ERC Instrument for the Chemical composition of Aerosols) and trace gas instruments, combined with Lagrangian modeling simulation from CLaMS (Chemical Lagrangian Model of the Stratosphere) (e.g., Pommrich et al. (2014) and references therein) to study and investigate the pathways, persistence, and chemical processing of the particles originating from the ASM region. This study provides an important opportunity to advance our understanding of the strong influence of the ASM on the composition of ExLS aerosols by comparing measurements from the early (summer) and late (autumn) phases of the PHILEAS campaign, along with the implications for stratospheric chemistry and the Earth's climate system.

https://doi.org/10.5194/egusphere-2026-998
Preprint. Discussion started: 19 March 2026


## 2 Methods

### 2.1 PHILEAS Campaign

We performed airborne measurements of aerosol and trace gases in the extratropical UTLS region in August and September 2023 (Fig. 1; Riese et al., 2025). The instrument platform was the German research aircraft HALO, enabling flight altitudes of up to 15 km and to a highest potential temperature of 405 K during the campaign. The PHILEAS mission was structured into three campaign phases. The first phase involved sampling of air masses over Europe, the Mediterranean region, and West Asia, with the base of operations at Oberpfaffenhofen, Germany. The second phase focused on measurements over North America and the North Pacific region, operating out of Anchorage, Alaska. The third and final phase returned to Europe for additional sampling, with the base again at Oberpfaffenhofen, Germany. During the campaign the aircraft was equipped with several aerosol and trace gas instruments, which are explained in detail below.

Previous studies using the Chemical Lagrangian Model of the Stratosphere (CLaMS) have consistently demonstrated the pronounced seasonal influence of Asian boundary layer emission on the ExLS composition (Vogel et al., 2016, 2019). It was shown that artificial tracers originating from South Asia and the western Pacific gradually increase in the ExLS from late spring onward. Maximum contributions typically occur during late summer and early autumn. This seasonal behavior has been documented for multiple years, highlighting the robustness independent of individual years (Graßl et al., 2024; Ploeger et al., 2017; Vogel et al., 2016, 2019). In particular, Vogel et al. (2016) provide a representative example of this temporal evolution, showing a gradual buildup of Asian surface emission tracers in the Northern Hemisphere ExLS throughout the monsoon season, followed by sustained elevated contributions into early autumn. Although the analysis is based on 2012 simulations, the results serve as a conceptual framework for distinguishing different phases of the influence of the ASM on the ExLS rather than as a description specific to 2012. Based on these earlier modeling studies, we differentiate here between measurements conducted during the so-called Early Phase (mid-August 2023) and Late Phase (late September 2023). This phase separation allows us to examine the seasonal contribution of Asian boundary layer emissions on the stratospheric aerosol composition during the PHILEAS campaign. In detail, we analyzed data from the following flights: F04, F06, and F07 (mid-August), summarized as the 'Early Phase', and F18, F19, and F20 (late September), referred to as the 'Late Phase'. The corresponding flight tracks are shown in Fig. 1. In the following, we compare aerosol and trace gas measurements taken during these two phases to analyze changes in the stratospheric background composition between summer and autumn (after the break-up of the AMA). Further details on the sampling strategy and information about the PHILEAS campaign can be found in Riese et al. (2025).

https://doi.org/10.5194/egusphere-2026-998
Preprint. Discussion started: 19 March 2026


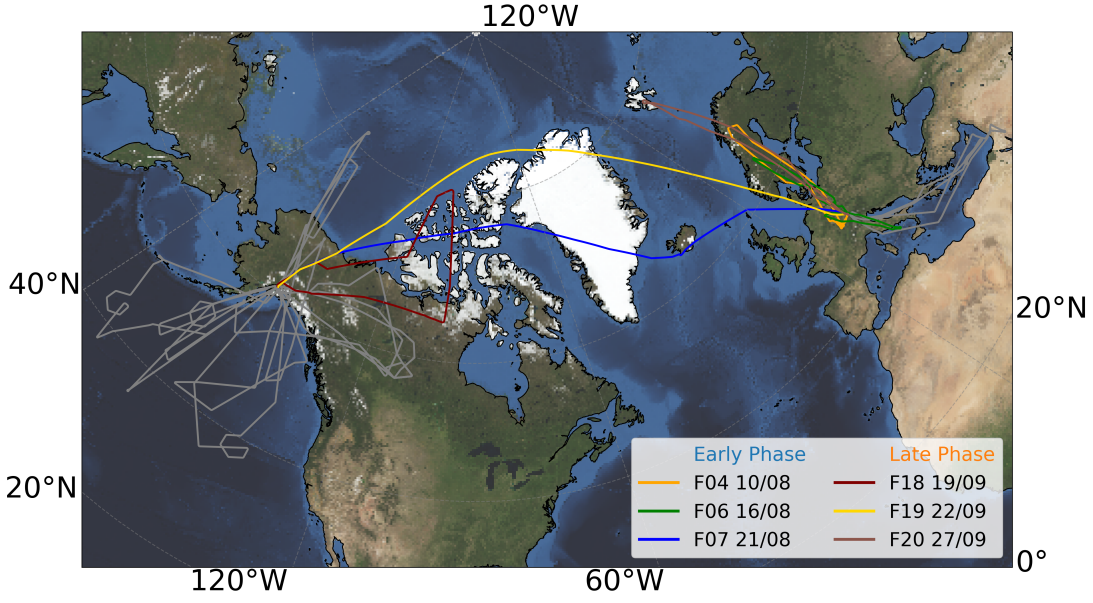


**Figure 1.** Flight paths of the six research flights during the PHILEAS campaign in 2023 that are relevant for this study (colored). Flights F04, F06, and F07 (mid-August) are grouped as the 'Early Phase' while Flights F18, F19, and F20 (late September) represent the 'Late Phase'. Grey lines represent other flight paths from the PHILEAS campaign to illustrate the full spatial and temporal coverage of the measurements.

## 2.2 Instrumentation

### 2.2.1 ERICA-LAMS: Measurement technique and particle classification

To capture information on the submicron aerosol composition, the ERICA instrument was deployed on the HALO aircraft during PHILEAS 2023 (Hünig et al., 2022; Dragoneas et al., 2022). We used the HASI (HALO Aerosol Submicrometer Inlet) system to sample air masses outside the aircraft in flight direction (Minikin et al., 2017; Andreae et al., 2018). The inlet was used in combination with the HASI Flow Control Unit (FCU). The FCU controls the flows in the inlet system to provide isokinetic sampling. An additional bypass pump was deployed to maintain an isokinetic flow to the ERICA instrument. Further details about the flow system can be found in the Supplementary Information (Sect. S1).

The measurement principle of the ERICA instrument is briefly described in the following. Particles enter the system through a constant-pressure inlet, maintaining a constant pressure within the aerodynamic lens by a varying volume flow into the instrument (Molleker et al., 2020). Subsequently, the particles are focused to a narrow beam with the help of the aerodynamic lens (Zhang et al., 2002b; Peck et al., 2016; Xu et al., 2017). After passing the lens, the particles are detected by two light scattering signals ($\lambda = 405$ nm), allowing the measurement of the size-dependent particle velocity. We used manufactured polystyrene latex particles of different sizes to calibrate and determine the vacuum-aerodynamic diameter ($d_{va}$) of the atmospheric particles. In the next step, the particles enter the high-vacuum system. Here, with the ERICA-LAMS (Laser Ablation Mass Spectrometer) technique, the particles are ablated and ionized by single-triggered laser shots (frequency-quadrupled Nd:YAG laser with

https://doi.org/10.5194/egusphere-2026-998
Preprint. Discussion started: 19 March 2026


a wavelength of $\lambda$ = 266 nm and an energy between 3.8 mJ to 4.5 mJ). The resulting positive and negative ions are extracted by electrical fields to generate bipolar mass spectra for each individual aerosol particle. Overall, this technique provides information on the single particle chemical composition, the mixing state, and the size of individual particles. This technique further enables the differentiation between refractory and non-refractory components within each aerosol particle. Due to the limitations of the aerodynamic lens and the detection unit, the ERICA-LAMS covers a particle size range from approximately 180 nm to 3000 nm (Hünig et al., 2022).

A total of 37,401 single-particle spectra obtained from ERICA-LAMS were analyzed using the CRISP software package (Concise Retrieval of Information from Single Particles; Klimach, 2012). The analysis involved the calibration of the ion mass-to-charge ratio ($m/z$ ratio) for each spectrum, followed by the classification of particle mass spectra into certain types. In this context, $NO^+$-rich particles were identified by a predominant ion signal at $m/z$ +30 corresponding to $NO^+$, following the methodology outlined in Appel et al. (2022), in which this particle type was named 'secondary Type 1'. Additionally, we differentiated between primary and secondary particle components present within the $NO^+$-rich particles, as described in Appel et al. (2022). For this study, we limit the size range of the secondary type $NO^+$-rich particles to between 200 and 500 nm ($d_{va}$), which reflects ~94 % and ~86% of the particles for the StratoClim and PHILEAS missions, respectively. We excluded larger and smaller particles sizes from the evaluation due to the effect of particle size on the ratio of ion peak intensities (Supplementary Information Sect. S2.4). The average spectrum of the $NO^+$-rich particle type for the Early and Late Phase is given in Fig. 2. Furthermore, potassium-dominated particles were identified by a pronounced $K^+$ ion signal at $m/z$ +39/+41, which is characteristic of biomass burning (BB) sources (e.g., Schill et al. 2020; Hudson et al. 2004; Bi et al. 2011). The denotation $NO^+$-rich and potassium-dominated used in this study refers to the comparatively strong signal intensities of $NO^+$ and $K^+$. It does not imply that the particles consist exclusively of these components, since minor contributions from organic material, sulfate, and others can also be present (Fig. 2 and S3). The particle fraction (PF) for each particle type was calculated by binning the number of particles of each type relative to the total number of particles within 5 K potential temperature and 5° equivalent latitude intervals. Comprehensive details regarding the ERICA-LAMS data post-processing and analysis are provided in the Supplementary Information Sect. S2.

https://doi.org/10.5194/egusphere-2026-998
Preprint. Discussion started: 19 March 2026


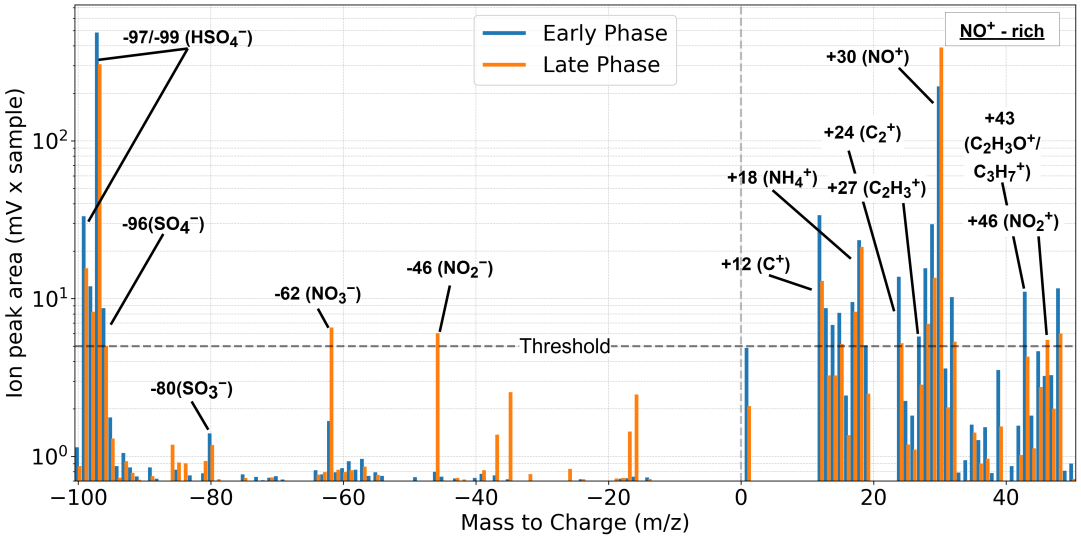


**Figure 2.** Bipolar mean spectra of the ERICA-LAMS $NO^+$-rich particle type: Comparison between the Early and Late Phases. The Early Phase average is based on 1,302 $NO^+$-rich particles, whereas the Late Phase average includes 9,182 $NO^+$-rich particles. In total, 10,484 $NO^+$-rich particles out of 37,401 analyzed aerosol particles were considered for this study, all of which were included in the ExLS background air mass during the Early and Late Phase. Further detailed information about the classification and threshold (5 mV * samples) of the spectra is given in the Supplementary Information Sect. S2.2 and S2.3.

In this study, we use the ratios and relative proportions of ion peak intensities in the average mass spectra of particle types to characterize the internal mixing state and composition of single particles (e.g. Bi et al., 2011; Healy et al., 2013, 2014; Shen et al., 2019). Table 1 summarizes particle types investigated in this study: $NO^+$-rich and potassium-dominated particles.

$NO^+$-rich particles are internally mixed with ammonium, nitrate, sulfate, and organic compounds (Fig. 2 and Tab. 1), consistent with earlier single particle measurements in the center of the AMA (StratoClim 2017 mission; Appel et al., 2022). To analyze the internal mixing state of $NO^+$-rich particles during PHILEAS, three key ion signal ratios were considered: the nitrate-to-sulfate ratio ($m/z$ −62/−97), the ammonium-to-nitrate ratio ($m/z$ +18/+30), and the ratio of less-to-more oxidized organic signals ($m/z$ +27/+43). These ratios were only calculated if both ion signals exceeded the respective ion marker threshold (>5mV x samples; see Supplementary Information Sect. S2.2), ensuring statistically significant interpretation.

https://doi.org/10.5194/egusphere-2026-998
Preprint. Discussion started: 19 March 2026


**Table 1.** This table shows characteristic and additional ion signals for two particle types relevant for this study, as well as their corresponding chemical species. The mean spectra of these particle types can be found in Fig. 2 and in Fig. S3 in the Supplementary Information.

| Particle type denotation | Characteristic ion signals in mean spectrum | Additional ion signals in mean spectrum | Corresponding chemical species |
|---|---|---|---|
| $NO^+$-rich[1] | *m/z* +30 ($NO^+$), +46 ($NO_2^+$), –46 ($NO_2^-$), –62 ($NO_3^-$) | *m/z* +18 ($NH_4^+$) | ammonium[5,6], nitrate[1,4,9] |
| | | $C^+_{1\text{-}2}$ | carbon ions[3,4,6,7,8,10] |
| | | *m/z* +27 ($C_2H_3^+$) | hydrocarbons[3,4,6,7,8,10] |
| | | *m/z* +43 ($C_3H_7^+$/$C_2H_3O^+$) | oxidized organics[3,4,6,7,8,10] |
| | | *m/z* –80 ($SO_3^-$), –96/–98 ($SO_4^-$), –97/–99 ($HSO_4^-$) | sulfate[4,6,8] |
| Potassium-dominated[2] | *m/z* +39/41 ($K^+$) | *m/z* +27 ($C_2H_3^+$), +37 ($C_3H^+$) | hydrocarbons[3,4,6,7,8,10] |
| | | *m/z* +43 ($C_3H_7^+$/$C_2H_3O^+$) | oxidized organics[3,4,6,7,8,10] |
| | | $C^+_{1\text{-}3}$ | carbon cluster ions[3,4,6,7,8,10] |
| | | *m/z* +23 ($Na^+$) | sodium[4,8] |
| | | *m/z* –26 ($CN^-$), –42 ($CNO^-$) | nitrogen-cont. organics[4,6,8] |
| | | *m/z* –80 ($SO_3^-$), –96/–98 ($SO_4^-$), –97/–99 ($HSO_4^-$) | sulfate[4,6,8] |

Literature for corresponding chemical species: 1: Adapted from Appel et al. (2022); 2: Adapted from Köllner et al. (2017); 3: Moffet et al. (2008); 4: Silva et al. (1999); 5: Noble and Prather (1996); 6: Pratt et al. (2011) 7: Spencer and Prather (2006); 8: Bi et al. (2011). 9: Murphy and Thomson (1997); 10: McGuire et al. (2011).

https://doi.org/10.5194/egusphere-2026-998
Preprint. Discussion started: 19 March 2026


### 2.2.2 ERICA-AMS

The second part of the instrument comprise the so-called ERICA-AMS (Aerosol Mass Spectrometer) technique. Here, non-refractory particle components, such as nitrate, sulfate, ammonium, and organic matter, are vaporized at around 600 °C on a tungsten vaporizer. The resulting vapor is then ionized by electron impact ionization. A compact time-of-flight mass spectrometer (C-TOF-MS) generates unipolar positive mass spectra of small particle ensembles with a time resolution of 10 s. The ERICA-AMS provides a quantitative analysis of the bulk chemical composition of these non-refractory aerosol components (Hünig et al., 2022). The ERICA system operates in alternating mode: during 5 s of laser ablation operation with ERICA-LAMS, the ERICA-AMS measures the background signal within the ionization chamber, which is closed by a shutter. It then switches to ERICA-AMS mode (with ERICA-LAMS in standby) to measure the aerosol beam for the following 5 s. This cycle repeats every 10 s.

The ERICA-AMS data were processed using TofWare 2.5.7 (Tofwerk), as detailed in Supplementary Information Sect. S3. For this study, 9,472 ERICA-AMS data points for each species corresponding to the Early and Late Phases of stratospheric background air masses were analyzed. Background noise calculations and detection limits for all species were performed following the methodology described by Appel et al. (2022), further information about the ERICA-AMS detection limits is provided in Supplementary Information Sect. S3.3. The average detection limits for the Early and Late Phases flights during this campaign, are summarized in Table 2.

**Table 2.** ERICA-AMS detection limits of each species averaged over the respective flights in the Early and Late Phase of PHILEAS ($\mu$g m$^{-1}$ at NTP: normal temperature (20 °C) and pressure (1013 hPa)). The detection limits are representative for a 10 s sampling interval.

| Detection Limit | Early Phase | Late Phase |
|---|---|---|
| Sulfate | 0.09 | 0.21 |
| Organic matter | 0.18 | 0.36 |
| Nitrate | 0.04 | 0.08 |
| Ammonium | 0.17 | 0.21 |

### 2.2.3 Trace Gas Measurements with UMAQS

The University of Mainz Airborne QCL-based Spectrometer (UMAQS) is an advanced instrument designed for precise in-situ measurements of trace gases, such as CO and nitrous oxide ($N_2O$), in the UTLS. Developed for atmospheric research, UMAQS operates with a temporal resolution of 1 s, enabling the detailed study of small-scale mixing and exchange processes across the tropopause. Utilizing quantum cascade laser (QCL) spectroscopy, UMAQS ensures high accuracy and reliability, as demonstrated during the PHILEAS campaign. We used the measurements of $N_2O$ and CO to identify stratospheric air masses, in particular stratospheric unperturbed air masses (see Sect. 2.3.2; Müller et al., 2016). Based on in-situ calibrations against

https://doi.org/10.5194/egusphere-2026-998
Preprint. Discussion started: 19 March 2026


secondary standards, which were calibrated against NOAA standards both before and after the campaign, the total uncertainty (2-sigma, 1 Hz) is estimated to be 0.3 ppbv for $N_2O$ and 1.4 ppbv for CO.

#### 2.2.4 Measurements of Cloud Hydrometers with the BCPD

The Backscatter Cloud Probe with Polarisation Detection (BCPD) was operated on HALO to identify the presence of cloud hydrometeors in the size range from 2 to 42 $\mu m$. The instrument detects particles by measuring light scattered in the backward direction and uses a polarization filter to distinguish between spherical and non-spherical shapes (Lucke et al., 2023). For PHILEAS, a cloud flag was derived from the BCPD based on the occurrence of particles within this size range that exceeded a number concentration of 0.02 $cm^{-3}$. Such signatures indicate the presence of liquid or mixed-phase cloud elements and were used to exclude cloud-contaminated periods from the aerosol analysis. This approach provides a robust indicator for cloud influence and served as the primary cloud flag throughout the PHILEAS dataset.

### 2.3 Modeling and Meteorology

#### 2.3.1 CLaMS Simulations

The CLaMS is a Lagrangian chemical transport model, with the advective transport scheme based on the calculation of three-dimensional forward trajectories and an additional parameterization of small-scale mixing based on deformations in the large-scale flow (e.g., Pommrich et al., 2014). The simulations for this paper have been driven with meteorological data from ERA5 reanalysis (Hersbach et al., 2020).

CLaMS simulations of surface origin tracers allow quantifying the amount of air originating from specific surface regions. In detail, surface origin tracers have been defined for different source regions (e.g., South Asia, western Pacific, entire Model Boundary Layer (MBL)). The definition of the regions is based on Vogel et al. (2025) and the origin tracer mixing ratios are set to unity in the lowest model layer (approximately the boundary layer) from 1st May on throughout the simulation. As these tracers are chemically inert, their mixing ratio at a given location and time equals the fraction of air originating in the respective surface region (for further details see Vogel et al., 2019, 2025).

A second CLaMS simulation provides information on the age of air spectra, the transit time distribution for an air mass since leaving the tropical surface (lowest model layer between 30 °N/S). The CLaMS-derived age spectra are calculated from pulse tracers in the model following Ploeger et al. (2021). The resolution of age spectra along the transit time axis is 1 month and therefore allows analysis of fast transport time scales into the UTLS, down to time scales of a few months. Both model diagnostics, including surface origin tracers as well as age of air spectra, have been interpolated along the PHILEAS research aircraft flight tracks to enable interpretation of the measurements.

Additionally, the diabatic CLaMS back trajectories were used to investigate also the origin and transport pathways of the air masses sampled during the PHILEAS campaign. These trajectories were driven by ERA5 reanalysis data with a horizontal resolution of 0.3° × 0.3° and were initialized along the flight paths at one-second resolution using aircraft positions. All trajectories were calculated backward in time until May 1, 2023, which allowed for the identification of source regions and

https://doi.org/10.5194/egusphere-2026-998
Preprint. Discussion started: 19 March 2026


transport histories on synoptic to seasonal timescales. The diabatical formulation provides a consistent representation of the transport process, which is particularly important for analyzing air mass pathways into the UTLS during the ASM. The back trajectory dataset follows the methodology described by Vogel et al. (2024) and Vogel et al. (2025) and complements the CLaMS surface origin tracers and age of air diagnostics by providing a Lagrangian perspective on individual air parcel histories.

### 2.3.2 Criteria for Identifying Stratospheric Background Air

Trace gases such as $N_2O$ and CO are commonly used to distinguish stratospheric air masses from tropospheric air and tropospheric pollution events (e.g., Müller et al., 2016; Joppe et al., 2024; Bönisch et al., 2009). In the troposphere, $N_2O$ exhibits almost uniform concentrations because of its long atmospheric lifetime and the absence of significant removal processes. In the stratosphere, however, $N_2O$ is gradually depleted by photolysis and reaction with excited oxygen atoms $O(^1D)$. As a result, mixing ratios decrease systematically with altitude and increasing potential temperature above the tropopause, allowing for an identification of stratospheric air masses (e.g., Zahn and Brenninkmeijer, 2003; Hegglin et al., 2006; Fischer et al., 2000).

During the PHILEAS campaign, stratospheric air was identified using a criterion of $N_2O$ mixing ratios being below 336 ppbv (Riese et al., 2025). In addition, air masses in the background stratosphere were further classified by applying a CO threshold of 40 ppbv, with CO serving as a tracer for pollution and combustion processes. The CO threshold was determined by analyzing the relative frequency distribution of all CO values measured in the stratosphere ($N_2O < 336$ ppbv; Fig. 3), which revealed two distinct modes representing undisturbed and polluted stratospheric air. Air masses with CO mixing ratios below this threshold are considered undisturbed by recent transport from polluted tropospheric air masses. The applied threshold is consistent with previous findings by Müller et al. (2016).

For the following analysis of CLaMS data, it is necessary to distinguish between unperturbed stratospheric and tropospheric air masses. To evaluate whether the $N_2O$ and CO thresholds, originally developed for in-situ measurements, are also usable to the CLaMS dataset, a comparison was made with potential vorticity (PV) values. The PV values derived from the ERA5 data (1°x1° resolution), which drive the CLaMS simulations, consistently exceed 7 PVU with major contribution from PV above 8 PVU when $N_2O$ and CO concentrations are below 336 ppbv and 40 ppbv, respectively. As a result, values above 8 PVU are consistent with the $N_2O$ and CO thresholds that were applied to the CLaMS data. Further, details on the PV threshold determination are provided in Supplementary Information Sect. S4.

https://doi.org/10.5194/egusphere-2026-998
Preprint. Discussion started: 19 March 2026


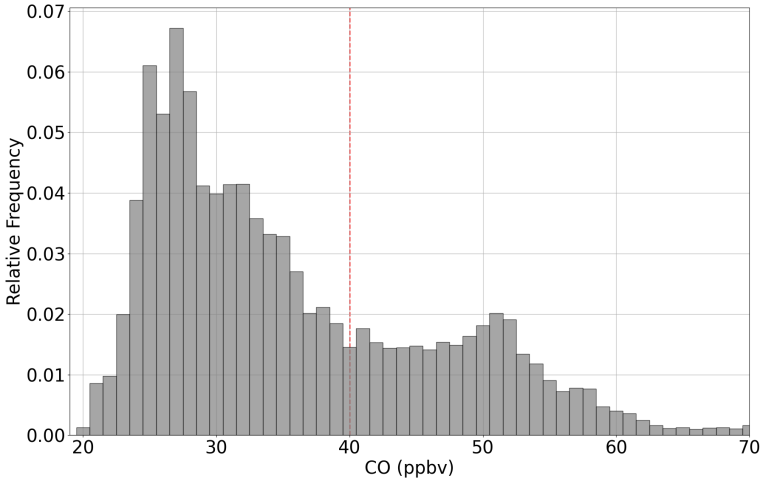


**Figure 3.** The relative frequency distribution of CO mixing ratios is based on data from all flights. Only data points with an $N_2O$ threshold of <336 ppbv for stratospheric signatures (Riese et al., 2025) were considered. The distribution exhibits two distinct regimes. A CO value of approximately 40 ppbv (red dashed line) was chosen as a practical separation point between these regimes. This threshold is consistent with the visual minimum between the two distributions and aligns well with ranges reported in previous studies (e.g., Müller et al., 2016). This threshold was used to differentiate between the undisturbed and polluted lower stratospheric air mass.

https://doi.org/10.5194/egusphere-2026-998
Preprint. Discussion started: 19 March 2026


## 3 Results and Discussion

The main objective of this section is to show that aerosol from the ASM region can affect the stratospheric background composition in the extratropics. First, we present in-situ particle composition measurements combined with CLaMS model results and compare the data for the two phases during PHILEAS (Early and Late Phase). Second, we demonstrate that the ExLS background composition in the Early Phase of PHILEAS was characterized by aerosol that could be associated with the ASM region. However, it was likely exposed to long residence time and chemical processing in the stratosphere.

### 3.1 Changes in ExLS Background Aerosol Composition Between Summer and Autumn

The ERICA-AMS measurements reveal significant changes in the particle composition in the ExLS background air from summer to autumn 2023. Figure 4 shows the difference in mean mass concentrations of nitrate, ammonium, and organic matter (as difference between the Late and Early Phase; defined in Fig. 1) as a function of potential temperature and equivalent latitude. The corresponding absolute concentrations as a function of potential temperature for both phases are also presented in Figure 4. A pronounced increase in nitrate and ammonium concentrations is observed in the Late Phase, particularly at potential temperatures above 370 K. Nitrate enhancements are most prominent between $40°$ and $60\,°\,\mathrm{N}$ equivalent latitude, reaching maximum values up to $0.06\,\mu\mathrm{g\,m^{-3}}$ (Fig. 4a, d). Along with nitrate, ammonium concentrations show increases above 370 K potential temperature with a maximum enhancement around $0.04\,\mu\mathrm{g\,m^{-3}}$ (Fig. 4b, e). In contrast, organic concentrations are decreasing from summer to autumn, particularly below 370 K potential temperature and at higher equivalent latitudes ($55°$ – $80\,°\,\mathrm{N}$) (Fig. 4c). The absolute organic mass concentrations shown in Fig. 4f indicate that organic matter concentration was consistently higher during the Early Phase compared to the Late Phase, which will be further examined in Sect. 3.1.2.

https://doi.org/10.5194/egusphere-2026-998
Preprint. Discussion started: 19 March 2026


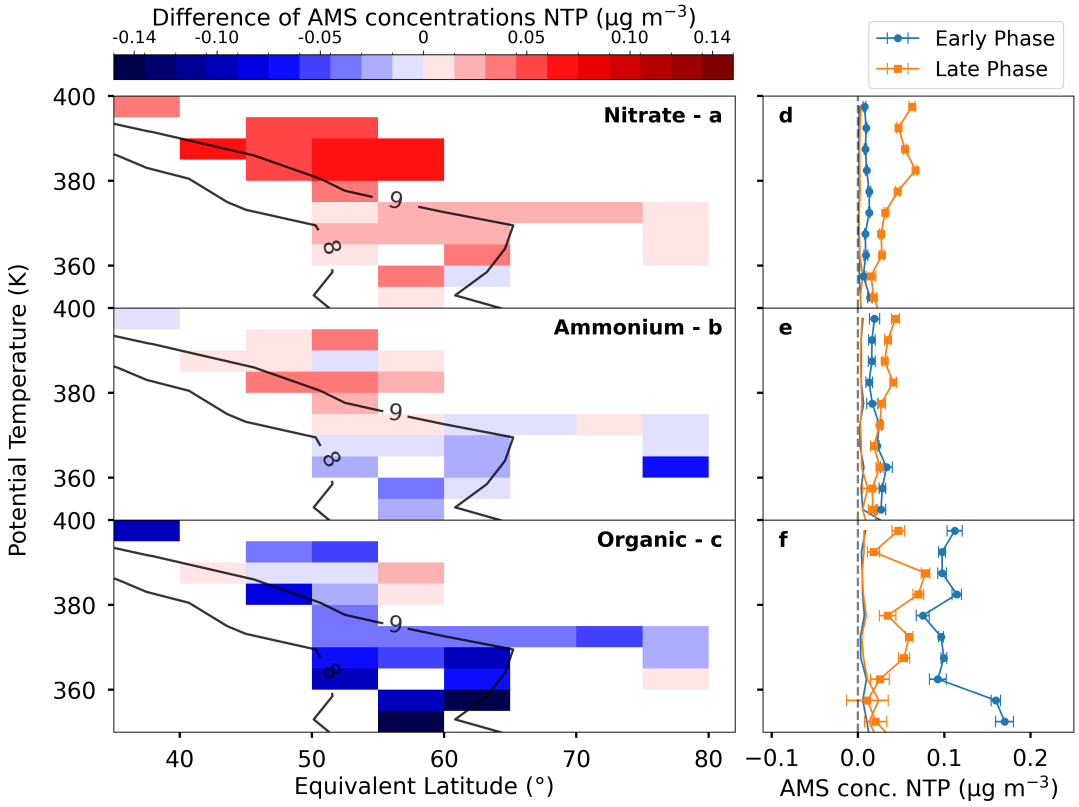


**Figure 4.** Mean distribution of ERICA-AMS nitrate (a), ammonium (b), and organic matter (c) mass concentrations shown as the difference between the Late and Early Phases (August and September), as a function of ERA5-derived equivalent latitude and potential temperature. Black contours indicate isolines of mean PV (ERA5-derived) in PVU. Panels (d–f) show the corresponding absolute mass concentrations of nitrate (d), ammonium (e), and organic matter (f) for the Early (blue) and Late (orange) Phases as a function of potential temperature. The vertical dashed line marks zero. The colored solid lines mark the detection limit for each potential temperature range and confirm the significance of the measurements. Details on the calculations, detection limits and uncertainties are provided in Supplementary Information S3.

The observed temporal evolution for nitrate and ammonium is further supported by the ERICA-LAMS data in Fig. 5. Figures 5a and b show the differences in PF of the $NO^+$-rich type and the potassium-dominated type between the Late and Early Phases, as a function of equivalent latitude and potential temperature. The data indicate a substantial increase in $NO^+$-rich PF during the summer-to-autumn transition, spanning over a broad spatial and vertical range (Fig. 5a). During the Early Phase, $NO^+$-rich particles made up less than 20% of the total particle population across the observed potential temperature range (Fig. 5 c). In contrast, during the Late Phase, their fractional abundance increased significantly, exceeding 20% and reaching almost 50% at approximately 380 K potential temperature (Fig. 5 c). These percentages refer to detectable particles, because pure sulfuric acid particles, which are common in the stratosphere, cannot be detected by the ERICA instrument. The mean mass spectrum of the $NO^+$-rich particle type (Fig. 2) indicates an internal mixture of nitrate, ammonium, sulfate, and organic matter.

https://doi.org/10.5194/egusphere-2026-998
Preprint. Discussion started: 19 March 2026


The results from the ERICA-LAMS single particle composition analysis (Fig. 5) are consistent with the observed increase in nitrate and ammonium detected by the ERICA-AMS (Fig. 4). A comparison of Figures 4a and 5a reveals that the fraction of $NO^+$-rich particles increases already at potential temperatures below 370 K, whereas enhanced nitrate mass concentrations are only observed above 370 K. This suggests that, although the PF of $NO^+$-rich particles increases below 370 K, these particles do not significantly contribute to the overall nitrate mass. A similar discrepancy between particle fraction and mass concentrations measured by ERICA-AMS and -LAMS has also been reported by Appel et al. (2022).

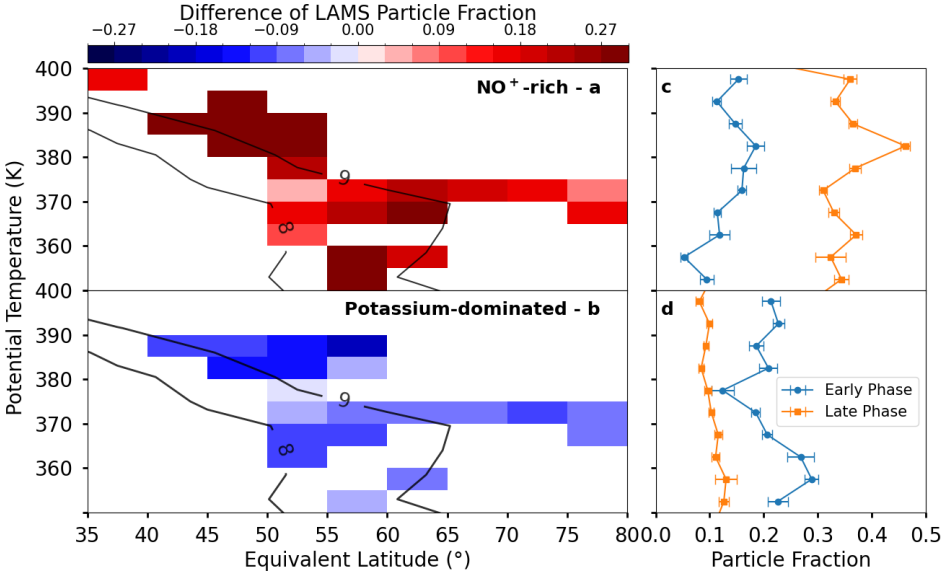


**Figure 5.** Mean distribution of ERICA-LAMS spectra based on the difference in particle fraction for $NO^+$-rich (a), potassium-dominated particles (b) between the Late and Early Phase, as a function of ERA5-derived equivalent latitude and potential temperature. The panel on the right shows the vertical profiles of PF for $NO^+$-rich (c), potassium-dominated particles (d) are shown for each phase. The black solid lines indicate isolines of PV (derived from ERA5) in PVU. Details on the uncertainties are provided in Supplementary Information S2.5.

### 3.1.1 Outflow from the ASM Drives the Increase of Nitrate and Ammonium in the ExLS in Autumn

The following findings provide evidence that the changes in stratospheric aerosol composition between summer and autumn are significantly influenced by the northward outflow of ASM-influenced air masses. First, the $NO^+$-rich particle type observed in this study closely resembles the particle type identified in the UTLS region over the ASM (within the ATAL) reported by Appel et al. (2022). In their study, it was demonstrated that particles containing ammonium nitrate are formed in the upper troposphere above the ASM convection. A key finding was that ammonium nitrate mass concentrations predominantly increased above 370 K potential temperature. Furthermore, they reported that aerosols in the ATAL primarily consist of nitrate, ammonium, and organic compounds, with nitrate concentrations exhibiting a pronounced peak between 370 K to 390 K. These results are in good agreement with our PHILEAS measurements, which reveal a similar increase in nitrate concentration and

https://doi.org/10.5194/egusphere-2026-998
Preprint. Discussion started: 19 March 2026


in the fraction of $NO^+$-rich particles at comparable potential temperature levels (see Fig. 4a,b and Fig. 5a). This consistency underscores the comparable chemical characteristics of aerosol populations observed during both campaigns.

Second, we analyzed CLaMS model results to investigate the origin and source regions of the enhanced particulate ammonium nitrate in the ExLS in autumn 2023. Figures 6 and 7 provide results from CLaMS surface-origin tracer and the CLaMS averaged age spectra as a comparison between the Early and Late Phases. The analysis reveals that the ExLS background air during the Late Phase, was influenced by recent transport of boundary layer air from the South Asia and western Pacific region (Fig. 6). The increase in the surface-origin tracer for the entire MBL between the Early and Late Phases indicates the growing influence of boundary layer air since the 1st May 2023 on the ExLS background air between autumn and summer 2023. Specifically, air masses from the South Asia and the western Pacific region contributed to the ExLS background composition during the Late Phase (Fig. 6).

Furthermore, the averaged CLaMS age spectra show differences in the ExLS background air between the Early and Late Phases (Fig. 7). The general shift in the age spectra between the Early and Late Phases reflects the time difference between the campaign phases, with the peaks at transit times of more than five months lagging by about one month in the Late Phase spectra compared to the Early Phase spectra. However, during the Late Phase in autumn, the ExLS background air exhibits a higher fraction of young air masses (<3.5 months; Fig. 7). In addition, Fig. 8 shows CLaMS-derived backward trajectory statistics for air masses observed during the Early Phase (Fig. 8a) and Late Phase (Fig. 8b). It is demonstrated that differences in backward trajectory points exists between the Early and Late Phases, indicating changes in the pre-dominant source regions and transport characteristics of young air masses reaching the ExLS. The Late Phase, in comparison to the Early Phase, exhibits a pronounced, spatially coherent maximum in trajectory density over northern India and along the southern margin of the Tibetan Plateau. This feature is accompanied by an increase in trajectory occurrence along the western and northern boundaries of the AMA, including regions in South and East Asia. The strong clustering of trajectory points during the Late Phase suggests that the AMA serves as an effective reservoir, holding ASM-influenced air masses for extended periods before exporting them poleward. It is thus obvious that the ExLS background air during the Late Phase was strongly influenced by relatively young (< 3.5 months) air masses from ground-level sources in South-East Asia. Furthermore, a recent study by Köllner et al. (2026) provides direct evidence for the northward transport of pollution aerosol (including ammonium nitrate) from the ASM region and irreversible mixing of this aerosol into the ExLS. The authors conclude that the quasi-horizontal isentropic advection occurring above 370 K potential temperature in the lower stratosphere is the most important transport pathway of pollution aerosol associated with the ASM region into the ExLS. In combination with their findings, this study provides additional evidence that polluted aerosol from Asia containing ammonium and nitrate are enriched in the ExLS background air and can persist there for a few months.

https://doi.org/10.5194/egusphere-2026-998
Preprint. Discussion started: 19 March 2026


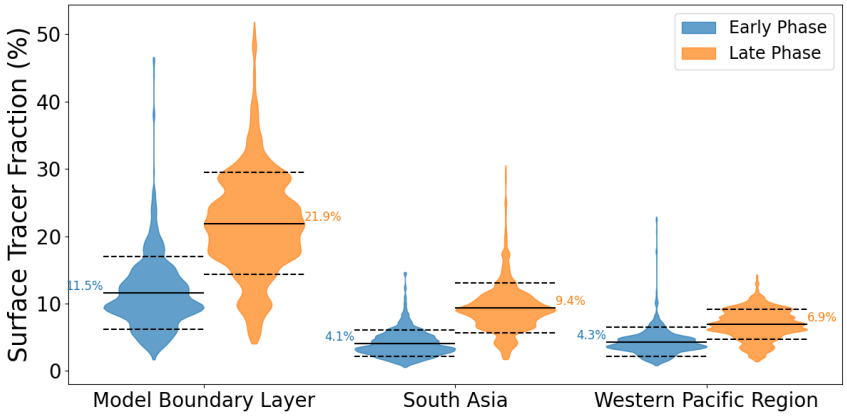


**Figure 6.** Violin plots of CLaMS-derived surface-origin tracer (%) from the MBL, South Asia, and the western Pacific region, comparing Early and Late Phases. Each violin is split into the Early Phase (left, blue) and the Late Phase (right, orange), with the solid horizontal bars indicating the mean value (annotated in % next to each bar) and the dashed lines marking standard deviation. The varying horizontal width of each violin represents the local data density, with wider areas corresponding to more frequent occurrences. Across all regions the Late Phase exhibits higher mean surface-origin tracer than the Early Phase (e.g., MBL early around 11.5 % compared to late around 21.9 %), reflecting an increase of boundary layer air from South Asia and the western Pacific into the ExLS towards autumn. The surface-origin tracers were filtered using the same thresholds as described in Sect. 2.3.2.

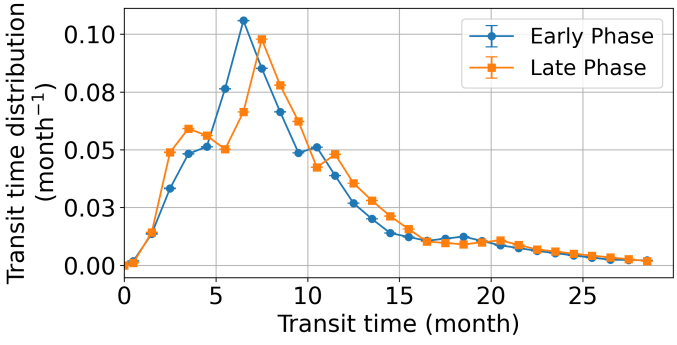


**Figure 7.** The CLaMS-derived age of air spectra are shown as averages over the Early (blue) and Late (orange) Phases, with the corresponding standard error of the mean values. This illustration shows the transit time distribution, indicating the fraction of air masses that have resided in the ExLS for a given period. The Early Phase exhibits an increases in the transit time distribution around 6.5, and 10.5 months. In the Late Phase, these features are still present but shifted toward about 7.5, and 11.5 months. The averaged CLaMS age of spectra were filtered using the same thresholds as described in Sect. 2.3.2.

For the complete analysis, backward trajectory statistics were also examined for potential temperatures below 320 K and above 380 K. These statistics reveal transport regimes. These layers are discussed in detail in the Supplement Section S5.

https://doi.org/10.5194/egusphere-2026-998
Preprint. Discussion started: 19 March 2026


Third, we observed a significant increase of methane ($CH_4$) and CO mixing ratios in the ExLS background air during the Late Phase. Figure 9 shows the probability density functions of both trace gases. Both trace gases can be related to tropospheric sources. In detail, enhanced CO mixing ratios are typically associated with combustion processes (e.g., Andreae and Merlet, 2001); $CH_4$ is mainly related to agricultural activity in Asia (e.g., Saunois et al., 2020). Earlier studies demonstrated that both trace gases show higher mixing ratios within AMA confined air masses (e.g., Lelieveld et al., 2018; Pan et al., 2016). In particular, Tomsche et al. (2019) demonstrated that $CH_4$ exhibits a pronounced and persistent enhancement within the ASM related air masses due to strong surface emissions and its long atmospheric lifetime, making it a robust tracer of ASM-influenced air masses in the UTLS. Previous studies have further shown that CO is an effective tracer for recently uplifted tropospheric air within the ASM dynamics and its subsequent export into the extratropical UTLS, particularly during late summer and early autumn (Müller et al., 2016). For $CH_4$ (Fig. 9a), the Late Phase exhibits a clear shift toward higher mixing ratios compared to the Early Phase. The Late Phase distribution primarily spans from 1850 to 1890 ppbv, while the Early Phase peaks at around 1820–1850 ppbv. This result reflects the accumulation of methane-rich air in the ExLS background air during autumn 2023. The CO distributions (Fig. 9b) show a similar pattern. Both phases overlap over a broad range, but the Late Phase is systematically shifted toward higher values. The maximum probability density in the Late Phase lies near 30–32 ppbv, while the Early Phase peaks closer to 27–29 ppbv. This concurrent shift toward higher mixing ratios of CO and $CH_4$ during the Late Phase provides further evidence for an enhanced influence of Asian boundary layer air on the ExLS background in autumn 2023.

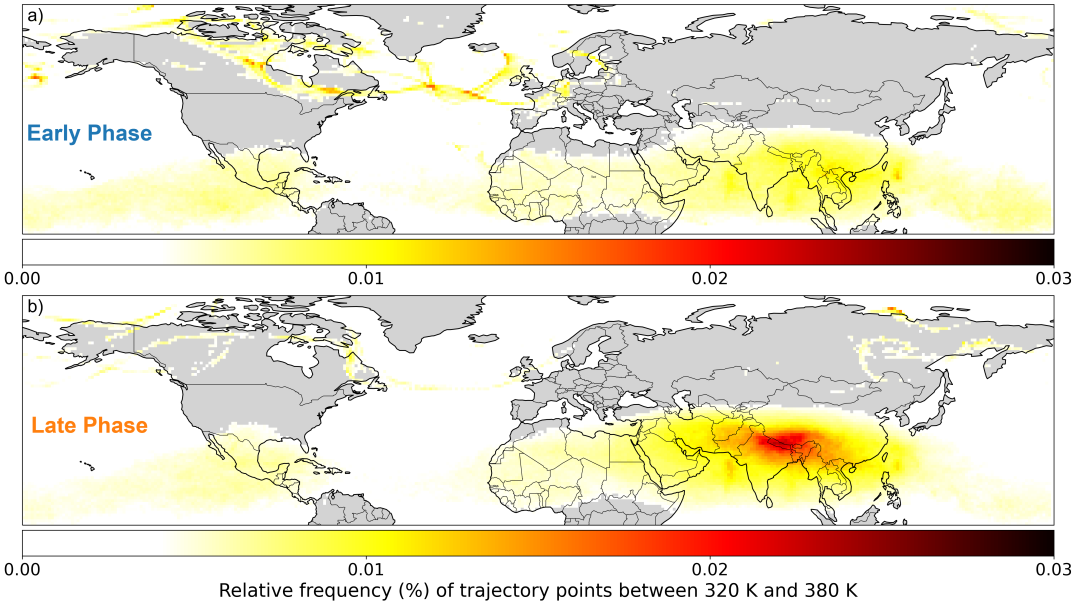


**Figure 8.** Relative frequency of CLaMS-derived backward trajectory end points between 320 K and 380 K potential temperature during the Early (a) and Late Phases (b) of the PHILEAS campaign. The data tracers were filtered using the same thresholds as described in Sect. 2.3.2

https://doi.org/10.5194/egusphere-2026-998
Preprint. Discussion started: 19 March 2026


Together, the observed changes of particulate ammonium nitrate in the ExLS background (above 370 K potential temperature) in autumn 2023 can be attributed to the presence of young air masses (<3.5 months) from Asian ground-level sources and its subsequent northward transport and outflow within the ASM circulation. This result is consistent with earlier studies, highlighting the ASM outflow as an important process to understand the increase of anthropogenic pollutants in the ExLS late summer and autumn (e.g., Bergman et al., 2013; Pan et al., 2016; Müller et al., 2016; Vogel et al., 2016; Fadnavis et al., 2024; Yu et al., 2015).

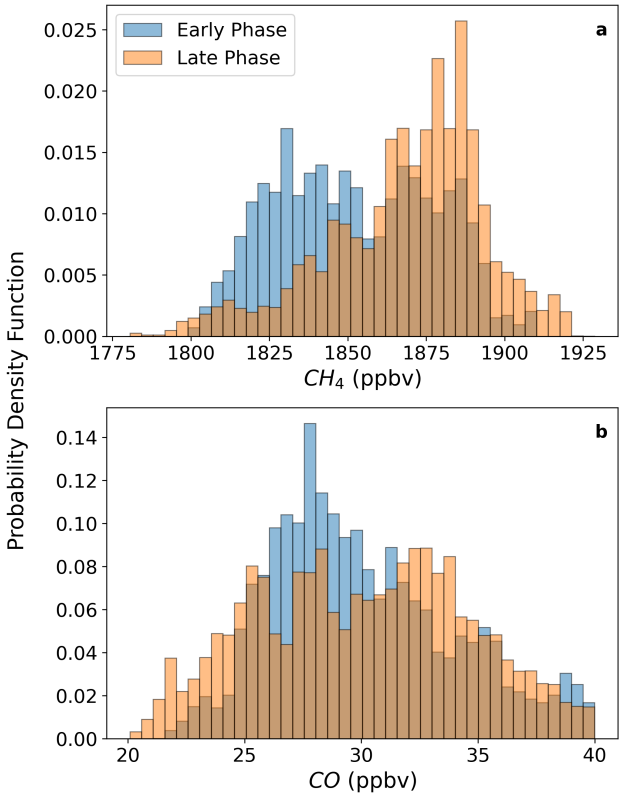


**Figure 9.** Probability density functions of measured $CH_4$ (a) and CO (b) mixing ratios during the Early (blue) and Late Phases (orange) of the PHILEAS campaign. The data were filtered using the same thresholds as described in Sect. 2.3.2.

https://doi.org/10.5194/egusphere-2026-998
Preprint. Discussion started: 19 March 2026


### 3.1.2 Biomass Burning Drives the Increase of Organic Matter in the ExLS in Summer

During the campaign, we observed a decrease in the concentration of particulate organics in the ExLS background air, particularly below a potential temperature of 370 K (Fig. 4 c). One reason for the observed changes in aerosol composition could be the declining influence of BB in the Northern Hemisphere in the course of the summer and autumn 2023. The Canadian wildfire season in 2023 was record-breaking with its unprecedented number of pyrocumulonimbus events between May and August (Zhang et al., 2024). However, Zhang et al. (2024) mentioned that stratospheric aerosol composition was not significantly perturbed by the pyrocumulonimbus events in 2023. In contrast, Katich et al. (2023) described that pyrocumulonimbus clouds can perturb stratospheric aerosol composition. Our measurements show that the ExLS background composition below 370 K was influenced by BB emissions during this Early Phase, as indicated by the abundance of organic matter (Fig. 4 c, f) and potassium-dominated particles (Fig. 5 b, d). Earlier studies showed that organic matter is largely enhanced in BB smoke observed in the stratosphere (e.g., Katich et al., 2023; Murphy et al., 2021; Martinsson et al., 2019). Potassium-dominated particles are known to originate from BB emissions (e.g., Hudson et al., 2004; Schill et al., 2020; Pratt et al., 2011). However, the PF of potassium-dominated particles progressively decreased from August (Early Phase) to September (Late Phase) (Fig. 5 b, d). This trend suggests a decreasing influence of BB emissions on the ExLS aerosol composition as well as a dilution and removal of BB-derived particles as the season advanced. Our observations are in line with measurements described by Martinsson et al. (2019), who reported a reduction in aerosol elemental concentration of carbon from August to September in the lowermost stratosphere.

Overall, our results provide evidence that the ASM outflow can alter the aerosol composition in the ExLS background air in summer/autumn. We observed the increasing abundance of ammonium nitrate in the ExLS background during the summer-to-autumn transitions. However, the organic content was likely dominated by BB events in summer (Early Phase of PHILEAS), rather than by the outflow from the ASM.

## 3.2 Changes in the Internal Mixing of $NO^+$-rich particles with residence time in the ExLS

This section compares the internal mixing state and chemical processing of $NO^+$-rich particles in four consecutive phases. First, we analyzed the $NO^+$-rich particles measured within the center of the AMA during the StratoClim 2017 mission in order to establish a reference for this particle type in close proximity to its source. Particularly, we analyzed the data below the 370 K potential temperature (defined as 'lower ATAL' in Appel et al., 2022), to study the $NO^+$-rich particles not affected by stratospheric air masses. Second, we analyzed $NO^+$-rich particles abundant in $CH_4$-rich stratospheric regimes in the extratropics measured during PHILEAS (defined as 'AMA filament in the ExLS'). This approach allows us to verify the internal mixing state and chemical processing of $NO^+$-rich particles under the influence of stratospheric air masses in narrow filaments detached from the AMA and recently introduced via quasi-horizontal advection into the ExLS. In detail, we selected the aerosol composition data in air masses with $CH_4 > 1920$ ppbv ($CH_4$-rich linked to Asian boundary layer sources - Tomsche et al., 2019; Köllner et al., 2026) and $N_2O < 336$ ppbv (stratospheric signature - Riese et al., 2025) from F08-F18 (focus on the western Pacific, northern Canada and Alaska region - Köllner et al., 2026). Third, we studied $NO^+$-rich particles observed in the ExLS

https://doi.org/10.5194/egusphere-2026-998
Preprint. Discussion started: 19 March 2026


background air (CO < 40 ppbv and $N_2O$ < 336 ppbv) during the Early Phase (mid-August) and Late Phase (late September) of the PHILEAS campaign. In this case, we selected data associated with CO < 40 ppbv and $N_2O$ < 336 ppbv to refer to to air masses of stratospheric signature combined with minor contribution from tropospheric pollution (including Asian boundary layer sources; for more details see Sect. 2.3.2). These four phases represent different extents of chemical processing during atmospheric transport and residence time, providing a framework for interpreting the evolution and mixing state of $NO^+$-rich particles from the center of the AMA into the ExLS.

For characterizing the particle mixing states, we specifically examined ratios of the ion signals at $m/z$ +30 ($NO^+$), -62 ($NO_3^-$), -97 ($HSO_4^-$ and other sulfate fragments), +27 ($C_2H_3^+$, less oxidized organics), and +43 ($C_2H_3O^+$ and other more oxidized organic fragments). The ratios of ammonium-to-nitrate, nitrate-to-sulfate, and less-to-more oxidized organic were chosen due to their sensitivity to compositional changes, stratospheric influence, and atmospheric oxidation processes, respectively. Additionally, Fig. 2 and Fig. S3 in Supplementary Information compare the differences in the ERICA-LAMS $NO^+$-rich particle mean spectra between the Early and Late Phase of the PHILEAS campaign.

Figure 10 illustrates the evolution of the internal mixing state of $NO^+$-rich particles across the four different phases. A comparison between the lower ATAL (StratoClim) and AMA filaments (PHILEAS) reveals a marked decrease of the nitrate-to-sulfate ratio and a slight increase of ammonium-to-nitrate ratio with increasing stratospheric residence time, indicating a relative enhancement of sulfate compared to nitrate. This change in the internal mixing state of $NO^+$-rich particles likely results from continued inclusion of sulfuric acid (via condensation and/or coagulation) along with the depletion of nitrate (e.g., Kremser et al., 2016; Junge and Manson, 1961; Murphy et al., 2014; Schneider et al., 2021). Further evidence to these conclusions comes from simulations with the global chemistry-climate model EMAC by Köllner et al. (2026). This study demonstrates that ammonium nitrate is replaced by ammonium(bi) sulfate with longer residence time of ammonium nitrate aerosol in the stratosphere. Between the AMA filaments and the Late Phase, both the nitrate-to-sulfate and the ammonium-to-nitrate ratios show only a slight change, suggesting that the change in the internal mixing state of $NO^+$-rich particles mainly occurs during the initial transition from upper tropospheric (lower ATAL) to stratospheric regimes.

The results in Fig. 10 further indicate that $NO^+$-rich particles measured in the ExLS during the Early Phase of PHILEAS were more chemically aged compared to particles measured in the upper troposphere in center of the AMA (lower ATAL). First, the ratio of less-to-more oxidized organic compounds decreased relative to the lower ATAL (StratoClim) reference, suggesting progressive organic oxidative aging while residing in the stratosphere (Fig. 10). Several studies have demonstrated the connection between photooxidative processes and increasing oxidation of organic aerosol components (e.g., O'Brien and Kroll, 2019; Zhao et al., 2022; Baboomian et al., 2020; Hu et al., 2021). We show that the degree of photochemical aging in $NO^+$-rich particles most likely increases with atmospheric residence time. The longer these particles remain in the atmosphere, the greater their exposure to oxidative processes, particularly under stratospheric conditions, resulting in a shift from less oxidized to more oxidized organic components.

Second, a significant increase in the ammonium-to-nitrate ratio from the Late to the Early Phase points to changes in the internal mixing state of $NO^+$-rich particles, with a shift toward lower nitrate and/or higher ammonium content. These distinct mixing state characteristics in the Early Phase are consistent with a prolonged stratospheric residence time, consistent to the

https://doi.org/10.5194/egusphere-2026-998
Preprint. Discussion started: 19 March 2026


CLaMS-derived age of air. Figure 7 shows that the Early and Late Phases exhibit similar transit time distributions, with a shift of approximately one month. The exception is a lower proportion of air masses with transit time less than five months during the Early Phase. Consequently, the Late Phase is predominantly influenced by the inflow of younger air masses (<5 months old), while the Early Phase is characterized by local maxima at approximately 6.5, 10.5, and 18.5 months. These findings suggest that the Early Phase is dominated by air masses that have resided in the stratosphere for several months to a year. This leads to enhanced chemical aging and probably includes remnants from the previous AMA season. Third, the ERICA-LAMS-derived particle size distribution of $NO^+$-rich particles (Fig. 11) shows a pronounced shift toward larger particle diameters during the Early Phase compared to both the Late Phase and the AMA filament. The size distribution of the Early Phase peaks at larger diameters and exhibits a broader mode, while the distributions for the AMA filaments and Late Phase are more narrowly centered at smaller particle sizes. This shift toward larger particle diameters in the Early Phase is consistent with progressive particle growth during prolonged stratospheric residence times. The broader and larger size mode further supports the conclusion that the $NO^+$-rich particles present during the Early Phase have undergone more chemical and microphysical aging in the stratospheric background. Taken together, the ERICA-LAMS ion signal ratios and CLaMS model data provide compelling evidence that the Early Phase of PHILEAS was dominated by chemically aged particles within the air masses of the ExLS background.

https://doi.org/10.5194/egusphere-2026-998
Preprint. Discussion started: 19 March 2026


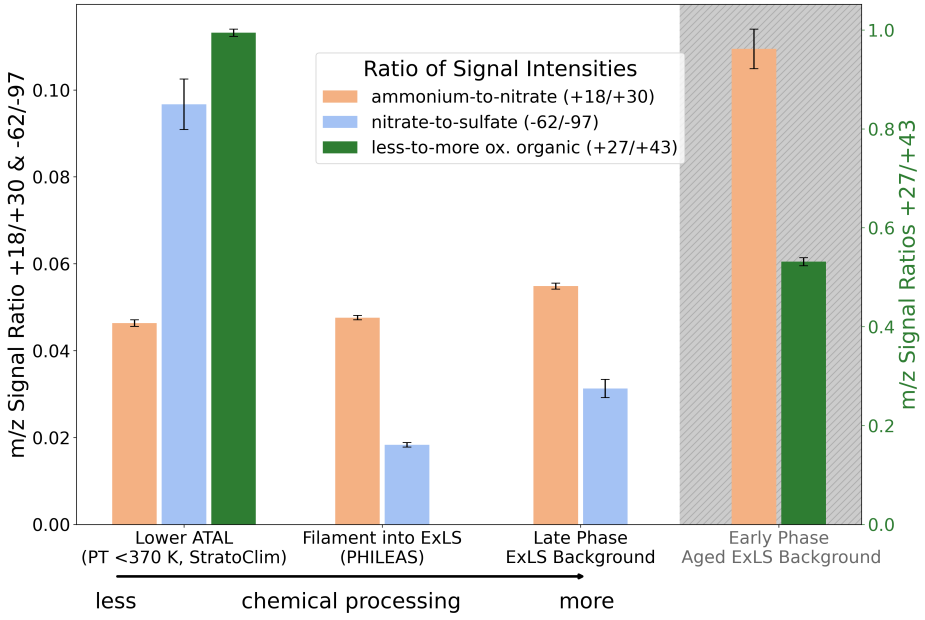


**Figure 10.** Ratios of key ion peaks in $NO^+$-rich particles across different PHILEAS phases. The green bar represents the ratio of less oxidized to more oxidized organic components, highlighting changes in organic composition over time. The orange bar represents the ammonium-to-nitrate signal intensity ratio. And the blue bar represents the nitrate-to-sulfate signal intensity ratio. The arrow at the bottom indicates the temporal evolution and chemical processing from $NO^+$-rich particles within the lower ATAL (StratoClim), AMA filaments into the ExLS, and Late Phase to the Early Phase, emphasizing how long term stratospheric residence alters particle composition. It was ensured that the mean value of the individual m/z signals exceeded the 5 mV * samples limit before the ratio calculation. More information about the uncertainty in Supplement Information Sect. S2.5

https://doi.org/10.5194/egusphere-2026-998
Preprint. Discussion started: 19 March 2026


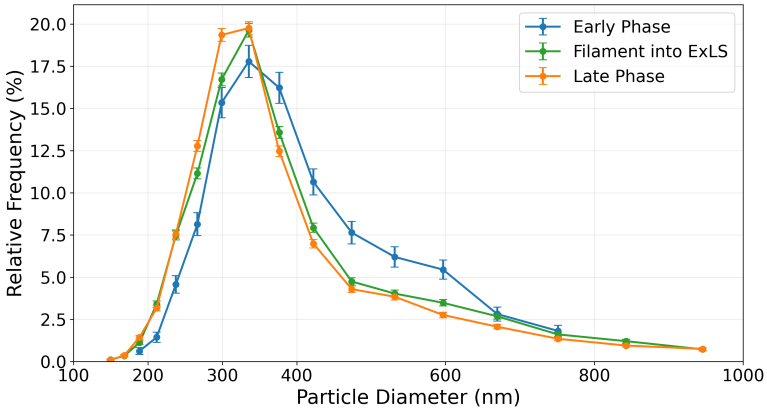


**Figure 11.** Particle size distribution (relative frequency) of $NO^+$-rich particles during the Early Phase (blue), AMA filament (green), and Late Phase (orange) of the PHILEAS campaign. The uncertainty bars represent the binomial standard deviation for relative frequencies and shows the statistical uncertainty for each size bin. As the detection efficiency of ERICA-LAMS can influence the indicated diameters, these size distributions represent relative rather than absolute particle sizes.

https://doi.org/10.5194/egusphere-2026-998
Preprint. Discussion started: 19 March 2026


## 4 Conclusions

Motivated by the limited knowledge of the ASM influence on the ExLS aerosol composition in summer and autumn, we performed aircraft-based measurements using the ERICA instrument with two complementary techniques. The ERICA-LAMS and ERICA-AMS provide data on the single particle composition and mixing state as well as on the bulk aerosol composition of non-refractory compounds, respectively. Our findings highlight a significant increase in ammonium nitrate aerosol concentrations within the ExLS background air mass from summer to autumn 2023, primarily driven by the northward transport of Asian boundary layer emissions in connection with the ASM circulation (see also Köllner et al., 2026).

In particular, enhanced nitrate and ammonium concentrations were observed during the Late Phase (late September), compared to the Early Phase (mid-August) of the PHILEAS mission. This increase coincided with a higher abundance of $NO^+$-rich aerosol particles measured by the ERICA-LAMS at equivalent latitudes between 40°N and 60°N and above 370 K potential temperature. Moreover, our observations align well with prior studies, particularly those from the StratoClim 2017 campaign (Appel et al., 2022), as indicated by the consistent detection of the characteristic $NO^+$-rich particle type in the ExLS.

The enhanced ammonium nitrate aerosol in the ExLS background air and the observed changes in aerosol composition can be interpreted through a combined analyses of ERICA aerosol compositions measurements and CLaMS modeling data. The CLaMS results suggest the transport of relatively young air masses (<3.5 months old) from the South Asian and western Pacific boundary layer regions into the ExLS, particularly in late summer and autumn of 2023. This finding is consistent with the observed increase in nitrate and ammonium aerosol concentrations and supports the assumption that the air masses entering the ExLS background originate from the ASM outflow dynamics. In contrast to ammonium nitrate, we observed a reduction in organic aerosol at the same equivalent latitudes but below 370 K, likely due to decreasing BB activities and possible dilution of BB air masses over the course of summer and autumn 2023. This is also reflected by the reduced abundance of potassium-dominated particles in these regions from summer to autumn. The interpretation is further supported by another study, showing the decreasing BB influence in the boreal region from summer to autumn 2023 (Zhang et al., 2024).

Our results further demonstrate that pollution aerosols, including ammonium nitrate, can persist in the lower stratosphere for several weeks until the end of September. While residing in the stratosphere, the particles undergo significant chemical processing, as evidenced by the change in the internal mixing state of $NO^+$-rich particles. We observed a decrease of the nitrate-to-sulfate ratio and a slight increase of the ammonium-to-nitrate ratio. This suggests that sulfate was included along with the depletion of nitrate in the lower stratosphere. Notably, the $NO^+$-rich particles detected in the Early Phase of the PHILEAS mission showed clear signs of chemical processing: a higher ammonium-to-nitrate ratio, a higher degree of oxidative aging of the organics, and increased particle sizes compared to the particles within the AMA. Combined with the findings from the CLaMS averaged age spectra, the air mass barely captures the signature of freshly mixed air masses. We thus hypothesize that the particles may remnants from the previous monsoon season. This would further indicates that the $NO^+$-rich particles can be observed in the stratosphere even after a few months with significant chemical processing.

https://doi.org/10.5194/egusphere-2026-998
Preprint. Discussion started: 19 March 2026


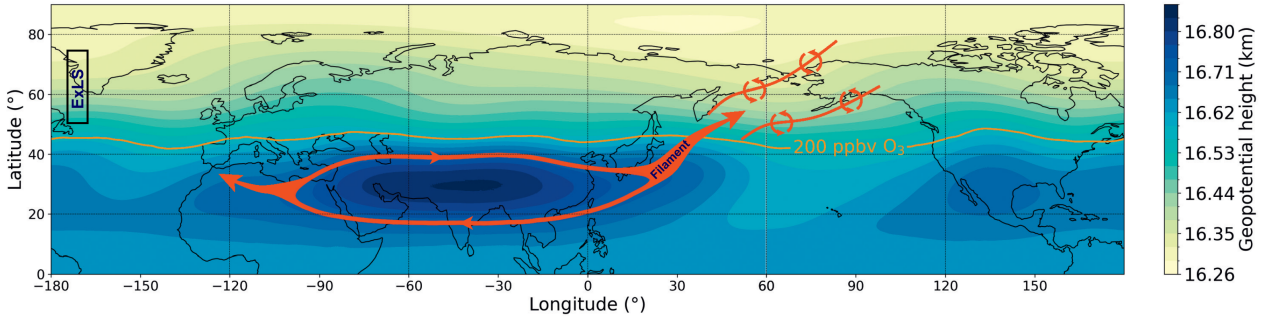


**Figure 12.** The illustration highlights the large-scale circulation of the AMA and its transport pathway toward the ExLS. It is based on averaged ERA5-derived geopotential height at 100 hPa from July to August 2023. The orange contour marks the region where ozone mixing ratios reach approximately 200 ppbv, indicating the transition toward the ExLS. Schematic arrows highlight the anticyclonic flow within the monsoon system, as well as the filamentary transport pathway that carries monsoon-influenced air masses towards higher latitudes, subsequently impacting the ExLS region. The cycle arrows demonstrate the filament mixing into the ExLS background.

Altogether, our study confirms the critical role of the ASM circulation as a significant pathway for transporting aerosols into the extratropical region, subsequently affecting the ExLS aerosol composition (as illustrated schematically in Fig. 12). The observed enrichment of ammonium nitrate aerosol within the ExLS may potentially impact radiative forcing and heterogeneous chemistry, processes crucial to stratospheric chemical composition and dynamics. However, our study faces limitations in temporal and spatial coverage, constraining the broader implications of our findings. Additional observational campaigns and extended monitoring are required to evaluate the year-to-year variability and the long-term role of ammonium nitrate aerosol in altering the chemical composition of the ExLS. For future research, we recommend detailed laboratory investigations into the chemical aging mechanisms of $NO^+$-rich particles to better understand their atmospheric evolution and the timescale for the chemical reactions. Additionally, exploring the contribution of ammonium nitrate aerosol to heterogeneous chemistry in the ExLS remains a critical next step. Finally, expanded observational datasets combined with global chemical transport modeling are essential for thoroughly assessing the contribution and climate implications of aerosol from the ASM region within the global stratospheric aerosol budget.

https://doi.org/10.5194/egusphere-2026-998
Preprint. Discussion started: 19 March 2026


*Data availability.* During the review process the data that supports our findings of this study are not publicly available. After acceptance, the data will be made openly accessible within a public repository with a DOI.

*Author contributions.* P.H., S.B., F.K., and J.S. designed the research project. F.E. developed the concept of the manuscript with the help of F.K.. F.E., O.E., J.S., A.D., S.M., P.B., and F.K. operated the ERICA instrument during the PHILEAS mission and/or supported the data acquisition during the PHILEAS aircraft campaign. F.E. with the help of F.K., O.E., and O.A. conducted the post-processing and preparation of the ERICA aerosol composition datasets. CLaMS data were provided by B.V. and F.P.. Flight planning, scientific discussion and data interpretation were supported by P.H., S.B., J.S., Y.C., M.E., H.C. C., and F.K.. L.T. provided the BCPD data. P.H., N.E., L.O., F.W., and H.C.L. provided the UMAQS data. F. E. wrote the manuscript with contributions from all coauthors. All authors reviewed and approved the final version of the results and interpretation.

*Competing interests.* The corresponding author confirms that there are no competing interests among the authors.

*Acknowledgements.* We gratefully acknowledge the support of the German Aerospace Center Flight Experiments (DLR-FX) for organizing the PHILEAS mission and operating HALO. Special thanks go to the pilots, engineers, technicians, and the entire operations team for their commitment throughout the campaign. We also thank the BAHAMAS team (DLR-FX) for operating the basic sensor suite on board HALO and providing essential data. Our appreciation extends to the flight planning team, especially Jens-Uwe Grooß, Christian Rolf, Rolf Müller, and Martin Riese, for their valuable expertise and support. We thank the European Centre for Medium-Range Weather Forecasts (ECMWF) for providing the ERA5 reanalyses data. We are grateful for the technical assistance provided by Rolf Maser and the enviscope team during the mission. The PHILEAS mission was funded by the Deutsche Forschungsgemeinschaft (DFG, German Research Foundation) (HALO-SPP 1294, project no: 461449927, HO 4225/17-1). The funding for individual projects within PHILEAS was provided by the DFG (KO 6470/1-1, HO 4225/19-1, HO 4120/4-1, VO 1276/7-1). The study was supported by TRR 301 'TPChange' (Project-ID 428312742). The design and construction of the ERICA instrument was funded by the ERC Advanced Grant 'EXCATRO' (FP7/2013-2019, grant no. 321040). We thank the mechanical and electronics workshops as well as the graphics department at the Max Planck Institute for Chemistry. We acknowledge the support and resources from the Particle Chemistry Department and the Aerosol Chemistry Department at the Max Planck Institute for Chemistry. We are grateful to Johannes Lucke (DLR) for helping to prepare the cloud flag data from the Backscatter Cloud Probe with Polarization Detection (BCPD). Finally, we appreciate the stimulating scientific discussions with Philipp Joppe, Thomas Klimach, and Mark Lamneck.

https://doi.org/10.5194/egusphere-2026-998
Preprint. Discussion started: 19 March 2026


## References

Andreae, M. O. and Merlet, P.: Emission of trace gases and aerosols from biomass burning, Global Biogeochemical Cycles, 15, 955–966, https://doi.org/https://doi.org/10.1029/2000GB001382, 2001.

Andreae, M. O., Afchine, A., Albrecht, R., Holanda, B. A., Artaxo, P., Barbosa, H. M. J., Borrmann, S., Cecchini, M. A., Costa, A., Dollner, M., Fütterer, D., Järvinen, E., Jurkat, T., Klimach, T., Konemann, T., Knote, C., Krämer, M., Krisna, T., Machado, L. A. T., Mertes, S., Minikin, A., Pöhlker, C., Pöhlker, M. L., Pöschl, U., Rosenfeld, D., Sauer, D., Schlager, H., Schnaiter, M., Schneider, J., Schulz, C., Spanu, A., Sperling, V. B., Voigt, C., Walser, A., Wang, J., Weinzierl, B., Wendisch, M., and Ziereis, H.: Aerosol characteristics and particle production in the upper troposphere over the Amazon Basin, Atmospheric Chemistry and Physics, 18, 921–961, https://doi.org/10.5194/acp-18-921-2018, 2018.

Annamalai, H. and Slingo, J. M.: Active break cycles: diagnosis of the intraseasonal variability of the Asian Summer Monsoon, Climate Dynamics, 18, 1432–0894, https://doi.org/10.1007/s003820100161, 2001.

Appel, O., Köllner, F., Dragoneas, A., Hünig, A., Molleker, S., Schlager, H., Mahnke, C., Weigel, R., Port, M., Schulz, C., Drewnick, F., Vogel, B., Stroh, F., and Borrmann, S.: Chemical analysis of the Asian tropopause aerosol layer (ATAL) with emphasis on secondary aerosol particles using aircraft-based in situ aerosol mass spectrometry, Atmospheric Chemistry and Physics, 22, 13 607–13 630, https://doi.org/10.5194/acp-22-13607-2022, 2022.

Baboomian, V. J., Gu, Y., and Nizkorodov, S. A.: Photodegradation of Secondary Organic Aerosols by Long-Term Exposure to Solar Actinic Radiation, ACS Earth and Space Chemistry, 4, 1078–1089, https://doi.org/10.1021/acsearthspacechem.0c00088, 2020.

Barth, M. C., Stuart, A. L., and Skamarock, W. C.: Numerical simulations of the July 10, 1996, Stratospheric-Tropospheric Experiment: Radiation, Aerosols, and Ozone (STERAO)-Deep Convection experiment storm: Redistribution of soluble tracers, Journal of Geophysical Research, 106, 12 381–12 400, https://doi.org/10.1029/2001JD900139, 2001.

Barth, M. C., Kim, S.-W., Skamarock, W. C., Stuart, A. L., Pickering, K. E., and Ott, L. E.: Simulations of the redistribution of formaldehyde, formic acid, and peroxides in the 10 July 1996 Stratospheric-Tropospheric Experiment: Radiation, Aerosols, and Ozone deep convection storm, Journal of Geophysical Research, 112, D13 310, https://doi.org/10.1029/2006JD008046, 2007a.

Barth, M. C., Kim, S.-W., Wang, C., Pickering, K. E., Ott, L. E., Stenchikov, G., Leriche, M., Cautenet, S., Pinty, J.-P., Barthe, C., Mari, C., Helsdon, J. H., Farley, R. D., Fridlind, A. M., Ackerman, A. S., Spiridonov, V., and Telenta, B.: Cloud-scale model intercomparison of chemical constituent transport in deep convection, Atmospheric Chemistry and Physics, 7, 4709–4731, https://doi.org/10.5194/acp-7-4709-2007, 2007b.

Berberich, J., Jacoby, S. A., Michailoudi, G., Schwarz, J. P., Viciani, S., D'Amato, F., Bianchini, G., Barucci, M., Campos, T., Ullman, K., Podolske, J. R., Gurganus, C., Smith, W. P., Ueyama, R., Honomichl, S. B., Pan, L. L., Woods, S., Wienzierl, B., Dollner, M., and Perring, A. E.: Black Carbon Reflects Extremely Efficient Aerosol Wet Removal in Monsoonal Convective Transport, Journal of Geophysical Research: Atmospheres, 130, e2024JD042 692, https://doi.org/https://doi.org/10.1029/2024JD042692, e2024JD042692 2024JD042692, 2025.

Bergman, J. W., Fierli, F., Jensen, E. J., Honomichl, S., and Pan, L. L.: Boundary layer sources for the Asian anticyclone: Regional contributions to a vertical conduit, Journal of Geophysical Research: Atmospheres, 118, 2560–2575, https://doi.org/https://doi.org/10.1002/jgrd.50142, 2013.

https://doi.org/10.5194/egusphere-2026-998
Preprint. Discussion started: 19 March 2026


Bi, X., Zhang, G., Li, L., Wang, X., Li, M., Sheng, G., Fu, J., and Zhou, Z.: Mixing state of biomass burning particles by single particle aerosol mass spectrometer in the urban area of PRD, China, Atmospheric Environment, 45, 3447–3453, https://doi.org/10.1016/j.atmosenv.2011.03.034, 2011.

Bian, J., Li, D., Bai, Z., Li, Q., Lyu, D., and Zhou, X.: Transport of Asian surface pollutants to the global stratosphere from the Tibetan Plateau region during the Asian summer monsoon, National Science Review, 7, 516–533, https://doi.org/10.1093/nsr/nwaa005, 2020.

Brunamonti, S., Jorge, T., Oelsner, P., Hanumanthu, S., Singh, B. B., Kumar, K. R., Sonbawne, S., Meier, S., Singh, D., Wienhold, F. G., Luo, B. P., Boettcher, M., Poltera, Y., Jauhiainen, H., Kayastha, R., Karmacharya, J., Dirksen, R., Naja, M., Rex, M., Fadnavis, S., and Peter, T.: Balloon-borne measurements of temperature, water vapor, ozone, and aerosol backscatter on the southern slopes of the Himalayas during StratoClim 2016–2017, Atmospheric Chemistry and Physics, 18, 15 937–15 957, https://doi.org/10.5194/acp-18-15937-2018, 2018.

Bönisch, H., Engel, A., Curtius, J., Birner, T., and Hoor, P.: Quantifying transport into the lowermost stratosphere using simultaneous in-situ measurements of SF6 and CO2, Atmospheric Chemistry and Physics, 9, 5905–5919, https://doi.org/10.5194/acp-9-5905-2009, 2009.

Clemens, J., Ploeger, F., Konopka, P., Portmann, R., Sprenger, M., and Wernli, H.: Characterization of transport from the Asian summer monsoon anticyclone into the UTLS via shedding of low potential vorticity cutoffs, Atmospheric Chemistry and Physics, 22, 3841–3860, https://doi.org/10.5194/acp-22-3841-2022, 2022.

Clemens, J., Vogel, B., Hoffmann, L., Griessbach, S., Thomas, N., Fadnavis, S., Müller, R., Peter, T., and Ploeger, F.: A multi-scenario Lagrangian trajectory analysis to identify source regions of the Asian tropopause aerosol layer on the Indian subcontinent in August 2016, Atmospheric Chemistry and Physics, 24, 763–787, https://doi.org/10.5194/acp-24-763-2024, 2024.

Dragoneas, A., Molleker, S., Appel, O., Hünig, A., Böttger, T., Hermann, M., Drewnick, F., Schneider, J., Weigel, R., and Borrmann, S.: The realization of autonomous, aircraft-based, real-time aerosol mass spectrometry in the upper troposphere and lower stratosphere, Atmospheric Measurement Techniques, 15, 5719–5742, https://doi.org/10.5194/amt-15-5719-2022, 2022.

Fadnavis, S., Roy, C., Chattopadhyay, R., Sioris, C. E., Rap, A., Müller, R., Kumar, K. R., and Krishnan, R.: Transport of trace gases via eddy shedding from the Asian summer monsoon anticyclone and associated impacts on ozone heating rates, Atmospheric Chemistry and Physics, 18, 11 493–11 506, https://doi.org/10.5194/acp-18-11493-2018, 2018.

Fadnavis, S., Sabin, T. P., Roy, C., Rowlinson, M., Rap, A., Vernier, J. P., and Sioris, C. E.: Elevated aerosol layer over South Asia worsens the Indian droughts, Scientific Reports, 9, 1–11, https://doi.org/10.1038/s41598-019-46704-9, 2019.

Fadnavis, S., Sonbawne, S. M., Laakso, A., Ploeger, F., Rap, A., Heinold, B., Sabin, T. P., and Müller, R.: Long range transport of South and East Asian anthropogenic aerosols counteracting Arctic warming, npj Climate and Atmospheric Science, 7, https://doi.org/10.1038/s41612-024-00633-1, 2024.

Fairlie, T. D., Liu, H., Vernier, J., Campuzano-Jost, P., Jimenez, J. L., Jo, D. S., Zhang, B., Natarajan, M., Avery, M. A., and Huey, G.: Estimates of Regional Source Contributions to the Asian Tropopause Aerosol Layer Using a Chemical Transport Model, Journal of Geophysical Research: Atmospheres, 125, e2019JD031 506, https://doi.org/10.1029/2019JD031506, 2020.

Fischer, H., Wienhold, F. G., Hoor, P., Bujok, O., Schiller, C., Siegmund, P., Ambaum, M., Scheeren, H. A., and Lelieveld, J.: Tracer correlations in the northern high latitude lowermost stratosphere: Influence of cross-tropopause mass exchange, Geophysical Research Letters, 27, 97–100, https://doi.org/10.1029/1999GL010879, 2000.

Fujiwara, M., Sakai, T., Nagai, T., Shiraishi, K., Inai, Y., Khaykin, S., Xi, H., Shibata, T., Shiotani, M., and Pan, L. L.: Lower-stratospheric aerosol measurements in eastward-shedding vortices over Japan from the Asian summer monsoon anticyclone during the summer of 2018, Atmospheric Chemistry and Physics, 21, 3073–3090, https://doi.org/10.5194/acp-21-3073-2021, 2021.

https://doi.org/10.5194/egusphere-2026-998
Preprint. Discussion started: 19 March 2026


Garny, H. and Randel, W. J.: Dynamic variability of the Asian monsoon anticyclone observed in potential vorticity and correlations with tracer distributions, Journal of Geophysical Research: Atmospheres, 118, 13,421–13,433, https://doi.org/https://doi.org/10.1002/2013JD020908, 2013.

Garny, H. and Randel, W. J.: Transport pathways from the Asian monsoon anticyclone to the stratosphere, Atmospheric Chemistry and Physics, 16, 2703–2718, https://doi.org/10.5194/acp-16-2703-2016, 2016.

Gettelman, A., Hoor, P., Pan, L. L., Randel, W. J., Hegglin, M. I., and Birner, T.: The extratropical upper troposphere and lower stratosphere, Reviews of Geophysics, 49, RG3003, https://doi.org/10.1029/2011RG000355, 2011.

Gottschaldt, K.-D., Schlager, H., Baumann, R., Cai, D. S., Eyring, V., Graf, P., Grewe, V., Jöckel, P., Jurkat-Witschas, T., Voigt, C., Zahn, A., and Ziereis, H.: Dynamics and composition of the Asian summer monsoon anticyclone, Atmospheric Chemistry and Physics, 18, 5655–5675, https://doi.org/10.5194/acp-18-5655-2018, 2018.

Graßl, S., Ritter, C., Tritscher, I., and Vogel, B.: Does the Asian summer monsoon play a role in the stratospheric aerosol budget of the Arctic?, Atmospheric Chemistry and Physics, 24, 7535–7557, https://doi.org/10.5194/acp-24-7535-2024, 2024.

Hanumanthu, S., Vogel, B., Müller, R., Brunamonti, S., Fadnavis, S., Li, D., Ölsner, P., Naja, M., Singh, B. B., Kumar, K. R., Sonbawne, S., Jauhiainen, H., Vömel, H., Luo, B., Jorge, T., Wienhold, F. G., Dirkson, R., and Peter, T.: Strong day-to-day variability of the Asian Tropopause Aerosol Layer (ATAL) in August 2016 at the Himalayan foothills, Atmospheric Chemistry and Physics, 20, 14 273–14 302, https://doi.org/10.5194/acp-20-14273-2020, 2020.

Healy, R. M., Sciare, J., Poulain, L., Crippa, M., Wiedensohler, A., Prévôt, A. S. H., Baltensperger, U., Sarda-Estève, R., McGuire, M. L., Jeong, C.-H., McGillicuddy, E., O'Connor, I. P., Sodeau, J. R., Evans, G. J., and Wenger, J. C.: Quantitative determination of carbonaceous particle mixing state in Paris using single-particle mass spectrometer and aerosol mass spectrometer measurements, Atmospheric Chemistry and Physics, 13, 9479–9496, https://doi.org/10.5194/acp-13-9479-2013, 2013.

Healy, R. M., Riemer, N., Wenger, J. C., Murphy, M., West, M., Poulain, L., Wiedensohler, A., O'Connor, I. P., McGillicuddy, E., Sodeau, J. R., and Evans, G. J.: Single particle diversity and mixing state measurements, Atmospheric Chemistry and Physics, 14, 6289–6299, https://doi.org/10.5194/acp-14-6289-2014, 2014.

Hegglin, M. I., Brunner, D., Peter, T., Hoor, P., Fischer, H., Staehelin, J., Krebsbach, M., Schiller, C., Parchatka, U., and Weers, U.: Measurements of NO, NOy, N2O, and O3 during SPURT: implications for transport and chemistry in the lowermost stratosphere, Atmospheric Chemistry and Physics, 6, 1331–1350, https://doi.org/10.5194/acp-6-1331-2006, 2006.

Hersbach, H., Bell, B., Berrisford, P., Hirahara, S., Horányi, A., Muñoz-Sabater, J., Nicolas, J., Peubey, C., Radu, R., Schepers, D., Simmons, A., Soci, C., Abdalla, S., Abellan, X., Balsamo, G., Bechtold, P., Biavati, G., Bidlot, J., Bonavita, M., De Chiara, G., Dahlgren, P., Dee, D., Diamantakis, M., Dragani, R., Flemming, J., Forbes, R., Fuentes, M., Geer, A., Haimberger, L., Healy, S., Hogan, R. J., Hólm, E., Janisková, M., Keeley, S., Laloyaux, P., Lopez, P., Lupu, C., Radnoti, G., de Rosnay, P., Rozum, I., Vamborg, F., Villaume, S., and Thépaut, J. N.: The ERA5 global reanalysis, Quarterly Journal of the Royal Meteorological Society, 146, 1999–2049, https://doi.org/10.1002/qj.3803, 2020.

Honomichl, S. B. and Pan, L. L.: Transport from the Asian Summer Monsoon Anticyclone Over the Western Pacific, Journal of Geophysical Research: Atmospheres, 125, e2019JD032 094, https://doi.org/10.1029/2019JD032094, 2020.

Höpfner, M., Ungermann, J., Borrmann, S., Wagner, R., Spang, R., Riese, M., Stiller, G., Appel, O., Batenburg, A. M., Bucci, S., Cairo, F., Dragoneas, A., Friedl-Vallon, F., Hünig, A., Johansson, S., Krasauskas, L., Legras, B., Leisner, T., Mahnke, C., Möhler, O., Molleker, S., Müller, R., Neubert, T., Orphal, J., Preusse, P., Rex, M., Saathoff, H., Stroh, F., Weigel, R., and Wohltmann, I.: Ammonium ni-

https://doi.org/10.5194/egusphere-2026-998
Preprint. Discussion started: 19 March 2026


trate particles formed in upper troposphere from ground ammonia sources during Asian monsoons, Nature Geoscience, 12, 608–612, https://doi.org/10.1038/s41561-019-0385-8, 2019.

Hsu, C. J. and Plumb, R. A.: Nonaxisymmetric Thermally Driven Circulations and Upper-Tropospheric Monsoon Dynamics, Journal of the Atmospheric Sciences, 57, 1255–1276, https://doi.org/10.1175/1520-0469(2000)057<1255:NTDCAU>2.0.CO;2, 1999.

Hu, W., Liu, D., Su, S., Ren, L., Ren, H., Wei, L., Yue, S., Xie, Q., Zhang, Z., Wang, Z., et al.: Photochemical Degradation of Organic Matter in the Atmosphere, Advanced Sustainable Systems, 5, 2100 027, https://doi.org/10.1002/adsu.202100027, 2021.

Hudson, P. K., Murphy, D. M., Cziczo, D. J., Thomson, D. S., de Gouw, J. A., Warneke, C., Holloway, J., Jost, H.-J., and Hübler, G.: Biomass-burning particle measurements: Characteristic composition and chemical processing, Journal of Geophysical Research: Atmospheres, 109, D23S27, https://doi.org/10.1029/2003JD004398, 2004.

Hünig, A., Appel, O., Dragoneas, A., Molleker, S., Clemen, H.-C., Helleis, F., Klimach, T., Köllner, F., Böttger, T., Drewnick, F., Schneider, J., and Borrmann, S.: Design, characterization, and first field deployment of a novel aircraft-based aerosol mass spectrometer combining the laser ablation and flash vaporization techniques, Atmospheric Measurement Techniques, 15, 2889–2921, https://doi.org/10.5194/amt-15-2889-2022, 2022.

Joppe, P., Schneider, J., Kaiser, K., Fischer, H., Hoor, P., Kunkel, D., Lachnitt, H.-C., Marsing, A., Röder, L., Schlager, H., Tomsche, L., Voigt, C., Zahn, A., and Borrmann, S.: The influence of extratropical cross-tropopause mixing on the correlation between ozone and sulfate aerosol in the lowermost stratosphere, Atmospheric Chemistry and Physics, 24, 7499–7522, https://doi.org/10.5194/acp-24-7499-2024, 2024.

Junge, C. E. and Manson, J. E.: Stratospheric Aerosol Studies, Journal of Geophysical Research, 66, 2163–2182, https://doi.org/10.1029/JZ066i007p02163, 1961.

Katich, J. M., Apel, E. C., Bourgeois, I., Brock, C. A., Bui, T. P., Campuzano-Jost, P., Commane, R., Daube, B., Dollner, M., Fromm, M., Froyd, K. D., Hills, A. J., Hornbrook, R. S., Jimenez, J. L., Kupc, A., Lamb, K. D., McKain, K., Moore, F., Murphy, D. M., Nault, B. A., Peischl, J., Perring, A. E., Peterson, D. A., Ray, E. A., Rosenlof, K. H., Ryerson, T., Schill, G. P., Schroder, J. C., Weinzierl, B., Thompson, C., Williamson, C. J., Wofsy, S. C., Yu, P., and Schwarz, J. P.: Pyrocumulonimbus affect average stratospheric aerosol composition, Science, 379, 815–820, https://doi.org/10.1126/science.add3101, 2023.

Khaykin, S. M., Godin-Beekmann, S., Keckhut, P., Hauchecorne, A., Jumelet, J., Vernier, J.-P., Bourassa, A., Degenstein, D. A., Rieger, L. A., Bingen, C., Vanhellemont, F., Robert, C., DeLand, M., and Bhartia, P. K.: Variability and evolution of the midlatitude stratospheric aerosol budget from 22 years of ground-based lidar and satellite observations, Atmospheric Chemistry and Physics, 17, 1829–1845, https://doi.org/10.5194/acp-17-1829-2017, 2017.

Klimach, T.: Chemische Zusammensetzung der Aerosole: Design und Datenauswertung eines Einzelpartikel-Laserablationsmassenspektrometers, Ph.D. thesis, Johannes Gutenberg University Mainz, https://doi.org/10.25358/openscience-4386, 2012.

Kremser, S., Thomason, L. W., von Hobe, M., Hermann, M., Deshler, T., Timmreck, C., Toohey, M., Stenke, A., Schwarz, J. P., Weigel, R., Fueglistaler, S., Prata, F. J., Vernier, J.-P., Schlager, H., Barnes, J. E., Antuña-Marrero, J.-C., Fairlie, D., Palm, M., Mahieu, E., Notholt, J., Rex, M., Bingen, C., Vanhellemont, F., Bourassa, A., Plane, J. M. C., Klocke, D., Carn, S. A., Clarisse, L., Trickl, T., Neely, R., James, A. D., Rieger, L., Wilson, J. C., and Meland, B.: Stratospheric aerosol—Observations, processes, and impact on climate, Reviews of Geophysics, 54, 278–335, https://doi.org/10.1002/2015RG000511, 2016.

https://doi.org/10.5194/egusphere-2026-998
Preprint. Discussion started: 19 March 2026


Köllner, F., Schneider, J., Willis, M. D., Klimach, T., Helleis, F., Bozem, H., Kunkel, D., Hoor, P., Burkart, J., Leaitch, W. R., Aliabadi, A. A., Abbatt, J. P. D., Herber, A. B., and Borrmann, S.: Particulate trimethylamine in the summertime Canadian high Arctic lower troposphere, Atmospheric Chemistry and Physics, 17, 13 747–13 766, https://doi.org/10.5194/acp-17-13747-2017, 2017.

Köllner, F., Kohl, M., Ekinci, F., Eppers, O., Schneider, J., Dragoneas, A., Molleker, S., Johansson, S., Ungermann, J., Kretschmer, E., Höpfner, M., Lauther, V., Volk, C. M., Appel, O., Brauner, P., Kunkel, D., Lachnitt, H.-C., Bozem, H., Weyland, F., Emig, N., Ort, L., Zahn, A., Tomsche, L., Pozzer, A., Lelieveld, J., Cheng, Y., Riese, M., Hoor, P., and Borrmann, S.: Aerosol from the Asian monsoon ubiquitous throughout the extratropical stratosphere, EarthArXiv, https://doi.org/10.31223/X5RB46, [prepint], 2026.

Lauther, V., Vogel, B., Wintel, J., Rau, A., Hoor, P., Bense, V., Müller, R., and Volk, C. M.: In situ observations of $CH_2Cl_2$ and $CHCl_3$ show efficient transport pathways for very short-lived species into the lower stratosphere via the Asian and the North American summer monsoon, Atmospheric Chemistry and Physics, 22, 2049–2077, https://doi.org/10.5194/acp-22-2049-2022, 2022.

Lawrence, M. G. and Lelieveld, J.: Atmospheric pollutant outflow from southern Asia: a review, Atmospheric Chemistry and Physics, 10, 11 017–11 096, https://doi.org/10.5194/acp-10-11017-2010, 2010.

Lelieveld, J., Bourtsoukidis, E., Brühl, C., Fischer, H., Fuchs, H., Harder, H., Hofzumahaus, A., Holland, F., Marno, D., Neumaier, M., Pozzer, A., Schlager, H., Williams, J., Zahn, A., and Ziereis, H.: The South Asian monsoon—pollution pump and purifier, Science, 361, 270–273, https://doi.org/10.1126/science.aar2501, 2018.

Lucke, J. R., Jurkat, T., Baumgardner, D., Kalinka, F., Moser, M., De La Torre Castro, E., and Voigt, C.: Characterization of Atmospheric Icing Conditions during the HALO-(AC) Campaign with the Nevzorov Probe and the Backscatter Cloud Probe with Polarization Detection, SAE Technical Paper, https://doi.org/10.4271/2023-01-1485, 2023.

Mahnke, C., Weigel, R., Cairo, F., Vernier, J. P., Afchine, A., Krämer, M., Mitev, V., Matthey, R., Viciani, S., D'Amato, F., Ploeger, F., Deshler, T., and Borrmann, S.: The Asian tropopause aerosol layer within the 2017 monsoon anticyclone: Microphysical properties derived from aircraft-borne in situ measurements, Atmospheric Chemistry and Physics, 21, 15 259–15 282, https://doi.org/10.5194/acp-21-15259-2021, 2021.

Martinsson, B. G., Friberg, J., Sandvik, O. S., Hermann, M., van Velthoven, P. F. J., and Zahn, A.: Formation and composition of the UTLS aerosol, npj Climate and Atmospheric Science, 2, 40, https://doi.org/10.1038/s41612-019-0097-1, 2019.

McGuire, M. L., Jeong, C.-H., Slowik, J. G., Chang, R. Y.-W., Corbin, J. C., Lu, G., Mihele, C., Rehbein, P. J. G., Sills, D. M. L., Abbatt, J. P. D., Brook, J. R., and Evans, G. J.: Elucidating determinants of aerosol composition through particle-type-based receptor modeling, Atmospheric Chemistry and Physics, 11, 8133–8155, https://doi.org/10.5194/acp-11-8133-2011, 2011.

Minikin, A., Sauer, D., Ibrahim, A., Franke, H., Röschenthaler, T., Fütterer, D., and Petzold, A.: The HALO Submicrometer Aerosol Inlet (HASI): Design Concept and First Characterization, poster presented at the HALO Symposium 2017, Oberpfaffenhofen, Germany, 2017.

Moffet, R. C., de Foy, B., Molina, L. T., Molina, M. J., and Prather, K. A.: Measurement of ambient aerosols in northern Mexico City by single particle mass spectrometry, Atmospheric Chemistry and Physics, 8, 4499–4516, https://doi.org/10.5194/acp-8-4499-2008, 2008.

Molleker, S., Helleis, F., Klimach, T., Appel, O., Clemen, H.-C., Dragoneas, A., Gurk, C., Hünig, A., Köllner, F., Rubach, F., Schulz, C., Schneider, J., and Borrmann, S.: Application of an O-ring pinch device as a constant-pressure inlet (CPI) for airborne sampling, Atmospheric Measurement Techniques, 13, 3651–3660, https://doi.org/10.5194/amt-13-3651-2020, 2020.

Murphy, D. M. and Thomson, D. S.: Chemical composition of single aerosol particles at Idaho Hill: Negative ion measurements, Journal of Geophysical Research: Atmospheres, 102, 6353–6368, https://doi.org/10.1029/96JD00859, 1997.

Murphy, D. M., Froyd, K. D., Schwarz, J. P., and Wilson, J. C.: Observations of the chemical composition of stratospheric aerosol particles, Quarterly Journal of the Royal Meteorological Society, 140, 1269–1278, https://doi.org/10.1002/qj.2213, 2014.

https://doi.org/10.5194/egusphere-2026-998
Preprint. Discussion started: 19 March 2026


Murphy, D. M., Froyd, K. D., Bourgeois, I., Brock, C. A., Kupc, A., Peischl, J., Schill, G. P., Thompson, C. R., Williamson, C. J., and Yu, P.: Radiative and chemical implications of the size and composition of aerosol particles in the existing or modified global stratosphere, Atmospheric Chemistry and Physics, 21, 8915–8932, https://doi.org/10.5194/acp-21-8915-2021, 2021.

Müller, S., Hoor, P., Bozem, H., Gute, E., Vogel, B., Zahn, A., Bönisch, H., Keber, T., Krämer, M., Rolf, C., Riese, M., Schlager, H., and Engel, A.: Impact of the Asian monsoon on the extratropical lower stratosphere: trace gas observations during TACTS over Europe 2012, Atmospheric Chemistry and Physics, 16, 10 573–10 589, https://doi.org/10.5194/acp-16-10573-2016, 2016.

Noble, C. A. and Prather, K. A.: Real-Time Measurement of Correlated Size and Composition Profiles of Individual Atmospheric Aerosol Particles, Environmental Science & Technology, 30, 2667–2680, https://doi.org/10.1021/es950669j, 1996.

Nützel, M., Dameris, M., and Garny, H.: Movement, drivers and bimodality of the South Asian High, Atmospheric Chemistry and Physics, 16, 14 755–14 774, https://doi.org/10.5194/acp-16-14755-2016, 2016.

O'Brien, R. E. and Kroll, J. H.: Photolytic aging of secondary organic aerosol: Evidence for a substantial photo-recalcitrant fraction, The Journal of Physical Chemistry Letters, 10, 4003–4009, https://doi.org/10.1021/acs.jpclett.9b01417, 2019.

Pan, L. L., Honomichl, S. B., Kinnison, D. E., Abalos, M., Randel, W. J., Bergman, J. W., and Bian, J.: Transport of chemical tracers from the boundary layer to stratosphere associated with the dynamics of the Asian summer monsoon, Journal of Geophysical Research: Atmospheres, 121, 14 159–14 174, https://doi.org/10.1002/2016JD025616, 2016.

Park, M., Randel, W. J., Emmons, L. K., Bernath, P. F., Walker, K. A., and Boone, C. D.: Chemical isolation in the Asian monsoon anticyclone observed in Atmospheric Chemistry Experiment (ACE-FTS) data, Atmospheric Chemistry and Physics, 8, 757–764, https://doi.org/10.5194/acp-8-757-2008, 2008.

Peck, J., Gonzalez, L. A., Williams, L. R., Xu, W., Croteau, P. L., Timko, M. T., Jayne, J. T., Worsnop, D. R., Miake-Lye, R. C., and Smith, K. A.: Development of an aerosol mass spectrometer lens system for PM2.5, Aerosol Science and Technology, 50, 781–789, https://doi.org/10.1080/02786826.2016.1190444, 2016.

Ploeger, F., Gottschling, C., Griessbach, S., Grooß, J.-U., Guenther, G., Konopka, P., Müller, R., Riese, M., Stroh, F., Tao, M., Ungermann, J., Vogel, B., and von Hobe, M.: A potential vorticity-based determination of the transport barrier in the Asian summer monsoon anticyclone, Atmospheric Chemistry and Physics, 15, 13 145–13 159, https://doi.org/10.5194/acp-15-13145-2015, 2015.

Ploeger, F., Konopka, P., Walker, K., and Riese, M.: Quantifying pollution transport from the Asian monsoon anticyclone into the lower stratosphere, Atmospheric Chemistry and Physics, 17, 7055–7066, https://doi.org/10.5194/acp-17-7055-2017, 2017.

Ploeger, F., Konopka, P., Grooß, J.-U., Günther, G., Müller, R., Pommrich, R., Livesey, N., Laube, J. C., Elvidge, E. C. L., Adcock, K. E., Baier, B., Brenninkmeijer, C. A. M., Chen, H., Droste, E. S., Heikkinen, P., Hind, A. J., Kivi, R., Lojko, A., Montzka, S. A., Oram, D. E., Randall, S., Röckmann, T., Sturges, W. T., Sweeney, C., Thomas, M., and Tuffnell, E.: Brewer–Dobson circulation and age of air in ERA5, Atmospheric Chemistry and Physics, 21, 8393–8412, https://doi.org/10.5194/acp-21-8393-2021, 2021.

Pommrich, R., Müller, R., Grooß, J.-U., Konopka, P., Ploeger, F., Vogel, B., Tao, M., Hoppe, C. M., Günther, G., Spelten, N., Hoffmann, L., Pumphrey, H.-C., Viciani, S., D'Amato, F., Volk, C. M., Hoor, P., Schlager, H., and Riese, M.: Tropical troposphere to stratosphere transport of carbon monoxide and long-lived trace species in the Chemical Lagrangian Model of the Stratosphere (CLaMS), Geoscientific Model Development, 7, 2895–2916, https://doi.org/10.5194/gmd-7-2895-2014, 2014.

Popovic, J. M. and Plumb, R. A.: Eddy Shedding from the Upper-Tropospheric Asian Monsoon Anticyclone, Journal of the Atmospheric Sciences, 58, 93–104, https://doi.org/10.1175/1520-0469(2001)058<0093:ESFTUT>2.0.CO;2, 2001.

https://doi.org/10.5194/egusphere-2026-998
Preprint. Discussion started: 19 March 2026


Pratt, K. A., Murphy, S. M., Subramanian, R., DeMott, P. J., Kok, G. L., Campos, T., Rogers, D. C., Prenni, A. J., Heymsfield, A. J., Seinfeld, J. H., and Prather, K. A.: Flight-based chemical characterization of biomass burning aerosols within two prescribed burn smoke plumes, Atmospheric Chemistry and Physics, 11, 12 549–12 565, https://doi.org/10.5194/acp-11-12549-2011, 2011.

Randel, W. J. and Park, M.: Deep convective influence on the Asian summer monsoon anticyclone and associated tracer variability observed with Atmospheric Infrared Sounder (AIRS), Journal of Geophysical Research: Atmospheres, 111, https://doi.org/https://doi.org/10.1029/2005JD006490, 2006.

Randel, W. J., Park, M., Emmons, L., Kinnison, D., Bernath, P., Walker, K. A., Boone, C., and Pumphrey, H.: Asian Monsoon Transport of Pollution to the Stratosphere, Science, 328, 611–613, https://doi.org/10.1126/science.1182274, 2010.

Riese, M., Hoor, P., Rolf, C., Kunkel, D., Vogel, B., Köllner, F., Pöhlker, M., Ploeger, F., Ungermann, J., Woiwode, W., Johansson, S., Bauer, R., Barmpounis, K., Borrmann, S., Brauner, P., Clemens, J., Dragoneas, A., Ekinci, F., Emig, N., Engel, A., Eppers, O., Fadnavis, S., Friedl-Vallon, F., Geldenhuys, M., Günther, G., Grooß, J., Hegglin, M., Höpfner, M., Jesswein, M., Joppe, P., Kaumanns, J., Kachula, O., Keber, T., Kretschmer, E., Lachnitt, H., Lauther, V., Lloyd, P., Molleker, S., Müller, R., Neubert, T., Ort, L., Pöschl, U., Pöhlker, C., Rapp, M., Retzlaff, M., Rhode, S., Schneider, J., Schuck, T., Sinnhuber, B., Spelten, N., Strobel, J., Tomsche, L., Turhal, K., van Luijt, R., Versick, S., Voigt, C., Volk, M., von Hobe, M., Weyland, F., Zahn, A., Ziereis, H., and Zlotos, L.: Long-range transport of polluted Asian summer monsoon air to high latitudes during the PHILEAS campaign in the boreal summer 2023, Bulletin of the American Meteorological Society, https://doi.org/10.1175/BAMS-D-24-0232.1, early Online Release, 2025.

Santee, M. L., Manney, G. L., Livesey, N. J., Schwartz, M. J., Neu, J. L., and Read, W. G.: A comprehensive overview of the climatological composition of the Asian summer monsoon anticyclone based on 10 years of Aura Microwave Limb Sounder measurements, Journal of Geophysical Research: Atmospheres, 122, 5491–5514, https://doi.org/https://doi.org/10.1002/2016JD026408, 2017.

Saunois, M., Stavert, A. R., Poulter, B., Bousquet, P., Canadell, J. G., Jackson, R. B., Raymond, P. A., Dlugokencky, E. J., Houweling, S., Patra, P. K., Ciais, P., Arora, V. K., Bastviken, D., Bergamaschi, P., Blake, D. R., Brailsford, G., Bruhwiler, L., Carlson, K. M., Carrol, M., Castaldi, S., Chandra, N., Crevoisier, C., Crill, P. M., Covey, K., Curry, C. L., Etiope, G., Frankenberg, C., Gedney, N., Hegglin, M. I., Höglund-Isaksson, L., Hugelius, G., Ishizawa, M., Ito, A., Janssens-Maenhout, G., Jensen, K. M., Joos, F., Kleinen, T., Krummel, P. B., Langenfelds, R. L., Laruelle, G. G., Liu, L., Machida, T., Maksyutov, S., McDonald, K. C., McNorton, J., Miller, P. A., Melton, J. R., Morino, I., Müller, J., Murguia-Flores, F., Naik, V., Niwa, Y., Noce, S., O'Doherty, S., Parker, R. J., Peng, C., Peng, S., Peters, G. P., Prigent, C., Prinn, R., Ramonet, M., Regnier, P., Riley, W. J., Rosentreter, J. A., Segers, A., Simpson, I. J., Shi, H., Smith, S. J., Steele, L. P., Thornton, B. F., Tian, H., Tohjima, Y., Tubiello, F. N., Tsuruta, A., Viovy, N., Voulgarakis, A., Weber, T. S., van Weele, M., van der Werf, G. R., Weiss, R. F., Worthy, D., Wunch, D., Yin, Y., Yoshida, Y., Zhang, W., Zhang, Z., Zhao, Y., Zheng, B., Zhu, Q., Zhu, Q., and Zhuang, Q.: The Global Methane Budget 2000–2017, Earth System Science Data, 12, 1561–1623, https://doi.org/10.5194/essd-12-1561-2020, 2020.

Schill, G. P., Froyd, K. D., Bian, H., Kupc, A., Williamson, C., Brock, C. A., Ray, E., Hornbrook, R. S., Hills, A. J., Apel, E. C., et al.: Widespread biomass burning smoke throughout the remote troposphere, Nature Geoscience, 13, 422—427, https://doi.org/10.1038/s41561-020-0586-1, 2020.

Schneider, J., Weigel, R., Klimach, T., Dragoneas, A., Appel, O., Hünig, A., Molleker, S., Köllner, F., Clemen, H.-C., Eppers, O., Hoppe, P., Hoor, P., Mahnke, C., Krämer, M., Rolf, C., Grooß, J.-U., Zahn, A., Obersteiner, F., Ravegnani, F., Ulanovsky, A., Schlager, H., Scheibe, M., Diskin, G. S., DiGangi, J. P., Nowak, J. B., Zöger, M., and Borrmann, S.: Aircraft-based observation of meteoric material in lower-stratospheric aerosol particles between 15 and 68°N, Atmospheric Chemistry and Physics, 21, 989–1013, https://doi.org/10.5194/acp-21-989-2021, 2021.

https://doi.org/10.5194/egusphere-2026-998
Preprint. Discussion started: 19 March 2026


Shen, X., Saathoff, H., Huang, W., Mohr, C., Ramisetty, R., and Leisner, T.: Understanding atmospheric aerosol particles with improved particle identification and quantification by single-particle mass spectrometry, Atmospheric Measurement Techniques, 12, 2219–2240, https://doi.org/10.5194/amt-12-2219-2019, 2019.

Silva, P. J., Liu, D.-Y., Noble, C. A., and Prather, K. A.: Size and Chemical Characterization of Individual Particles Resulting from Biomass Burning of Local Southern California Species, Environmental Science & Technology, 33, 3068–3076, https://doi.org/10.1021/es980544p, 1999.

Spencer, M. T. and Prather, K. A.: Using ATOFMS to Determine OC/EC Mass Fractions in Particles, Aerosol Science and Technology, 40, 585–594, https://doi.org/10.1080/02786820600729138, 2006.

Thomason, L. W. and Vernier, J.-P.: Improved SAGE II cloud/aerosol categorization and observations of the Asian tropopause aerosol layer: 1989–2005, Atmospheric Chemistry and Physics, 13, 4605–4616, https://doi.org/10.5194/acp-13-4605-2013, 2013.

Tomsche, L., Pozzer, A., Ojha, N., Parchatka, U., Lelieveld, J., and Fischer, H.: Upper tropospheric CH4 and CO affected by the South Asian summer monsoon during the Oxidation Mechanism Observations mission, Atmospheric Chemistry and Physics, 19, 1915–1939, https://doi.org/10.5194/acp-19-1915-2019, 2019.

Ungermann, J., Ern, M., Kaufmann, M., Müller, R., Spang, R., Ploeger, F., Vogel, B., and Riese, M.: Observations of PAN and its confinement in the Asian summer monsoon anticyclone in high spatial resolution, Atmospheric Chemistry and Physics, 16, 8389–8403, https://doi.org/10.5194/acp-16-8389-2016, 2016.

Vernier, H., Rastogi, N., Liu, H., Pandit, A. K., Bedka, K., Patel, A., Ratnam, M. V., Kumar, B. S., Zhang, B., Gadhavi, H., Wienhold, F., Berthet, G., and Vernier, J.-P.: Exploring the inorganic composition of the Asian Tropopause Aerosol Layer using medium-duration balloon flights, Atmospheric Chemistry and Physics, 22, 12 675–12 694, https://doi.org/10.5194/acp-22-12675-2022, 2022.

Vernier, J.-P., Thomason, L. W., Pommereau, J.-P., Bourassa, A., Pelon, J., Garnier, A., Hauchecorne, A., Blanot, L., Trepte, C., Degenstein, D., and Vargas, F.: Major influence of tropical volcanic eruptions on the stratospheric aerosol layer during the last decade, Geophysical Research Letters, 38, L12 807, https://doi.org/10.1029/2011GL047563, 2011.

Vernier, J.-P., Fairlie, T. D., Natarajan, M., Wienhold, F. G., Bian, J., Martinsson, B. G., Crumeyrolle, S., Thomason, L. W., and Bedka, K. M.: Increase in upper tropospheric and lower stratospheric aerosol levels and its potential connection with Asian pollution, Journal of Geophysical Research: Atmospheres, 120, 1608–1619, https://doi.org/10.1002/2014JD022372, 2015.

Vernier, J.-P., Fairlie, T. D., Deshler, T., Ratnam, M. V., Gadhavi, H., Kumar, B. S., Natarajan, M., Pandit, A. K., Raj, S. T. A., Kumar, A. H., Jayaraman, A., Singh, A. K., Rastogi, N., Sinha, P. R., Kumar, S., Tiwari, S., Wegner, T., Baker, N., Vignelles, D., Stenchikov, G., Shevchenko, I., Smith, J., Bedka, K., Kesarkar, A., Singh, V., Bhate, J., Ravikiran, V., Rao, M. D., Ravindrababu, S., Patel, A., Vernier, H., Wienhold, F. G., Liu, H., Knepp, T. N., Thomason, L., Crawford, J., Ziemba, L., Moore, J., Crumeyrolle, S., Williamson, M., Berthet, G., Jégou, F., and Renard, J.-B.: BATAL: The Balloon Measurement Campaigns of the Asian Tropopause Aerosol Layer, Bulletin of the American Meteorological Society, 99, 955–973, https://doi.org/10.1175/BAMS-D-17-0014.1, 2018.

Vogel, B., Günther, G., Müller, R., Grooß, J.-U., Hoor, P., Krämer, M., Müller, S., Zahn, A., and Riese, M.: Fast transport from Southeast Asia boundary layer sources to northern Europe: rapid uplift in typhoons and eastward eddy shedding of the Asian monsoon anticyclone, Atmospheric Chemistry and Physics, 14, 12 745–12 762, https://doi.org/10.5194/acp-14-12745-2014, 2014.

Vogel, B., Günther, G., Müller, R., Grooß, J.-U., and Riese, M.: Impact of different Asian source regions on the composition of the Asian monsoon anticyclone and of the extratropical lowermost stratosphere, Atmospheric Chemistry and Physics, 15, 13 699–13 716, https://doi.org/10.5194/acp-15-13699-2015, 2015.

https://doi.org/10.5194/egusphere-2026-998
Preprint. Discussion started: 19 March 2026


Vogel, B., Günther, G., Müller, R., Grooß, J.-U., Afchine, A., Bozem, H., Hoor, P., Krämer, M., Müller, S., Riese, M., Rolf, C., Spelten, N., Stiller, G. P., Ungermann, J., and Zahn, A.: Long-range transport pathways of tropospheric source gases originating in Asia into the northern lower stratosphere during the Asian monsoon season 2012, Atmospheric Chemistry and Physics, 16, 15 301–15 325, https://doi.org/10.5194/acp-16-15301-2016, 2016.

Vogel, B., Müller, R., Günther, G., Spang, R., Hanumanthu, S., Li, D., Riese, M., and Stiller, G. P.: Lagrangian simulations of the transport of young air masses to the top of the Asian monsoon anticyclone and into the tropical pipe, Atmospheric Chemistry and Physics, 19, 6007–6034, https://doi.org/10.5194/acp-19-6007-2019, 2019.

Vogel, B., Volk, C. M., Wintel, J., Lauther, V., Clemens, J., Grooß, J.-U., Günther, G., Hoffmann, L., Laube, J. C., Müller, R., Ploeger, F., and Stroh, F.: Evaluation of vertical transport in ERA5 and ERA-Interim reanalysis using high-altitude aircraft measurements in the Asian summer monsoon 2017, Atmospheric Chemistry and Physics, 24, 317–343, https://doi.org/10.5194/acp-24-317-2024, 2024.

Vogel, B., Lauther, V., Köllner, F., Ekinci, F., Rolf, C., Strobel, J., van Luijt, R., Volk, M. C., Borrmann, S., Dragoneas, A., Eppers, O., Molleker, S., Hoor, P., Ort, L., Weyland, F., Zahn, A., Clemens, J., Günther, G., Kachula, O., Müller, R., Ploeger, F., and Riese, M.: Continental and marine source regions contributing to the outflow of the Asian summer monsoon anticyclone during the PHILEAS campaign in summer 2023, EGUsphere, 2025, 1–49, https://doi.org/10.5194/egusphere-2025-5609, 2025.

Wagner, R., Bertozzi, B., Höpfner, M., Höhler, K., Möhler, O., Saathoff, H., and Leisner, T.: Solid Ammonium Nitrate Aerosols as Efficient Ice Nucleating Particles at Cirrus Temperatures, Journal of Geophysical Research: Atmospheres, 125, e2019JD032 248, https://doi.org/10.1029/2019JD032248, 2020.

Wang, X., Randel, W., Pan, L., Wu, Y., and Zhang, P.: Transient behavior of the Asian summer monsoon anticyclone associated with eastward eddy shedding, Journal of Geophysical Research: Atmospheres, 127, e2021JD036 090, https://doi.org/10.1029/2021JD036090, 2022.

Weigel, R., Mahnke, C., Baumgartner, M., Dragoneas, A., Vogel, B., Ploeger, F., Viciani, S., D'Amato, F., Bucci, S., Legras, B., Luo, B., and Borrmann, S.: In situ observation of new particle formation (NPF) in the tropical tropopause layer of the 2017 Asian monsoon anticyclone – Part 1: Summary of StratoClim results, Atmospheric Chemistry and Physics, 21, 11 689–11 722, https://doi.org/10.5194/acp-21-11689-2021, 2021.

Xenofontos, C., Kohl, M., Ruhl, S., Almeida, J., Beckmann, H. M., Caudillo-Plath, L., Ehrhart, S., Höhler, K., Kaniyodical Sebastian, M., Kong, W., Kunkler, F., Onnela, A., Rato, P., Russell, D. M., Simon, M., Stark, L., Umo, N. S., Unfer, G. R., Yang, B., Yu, W., Zauner-Wieczorek, M., Zgheib, I., Zheng, Z., Curtius, J., Donahue, N. M., El Haddad, I., Flagan, R. C., Gordon, H., Harder, H., He, X. C., Kirkby, J., Kulmala, M., Möhler, O., Pöhlker, M. L., Schobesberger, S., Volkamer, R., Wang, M., Borrmann, S., Pozzer, A., Lelieveld, J., and Christoudias, T.: The impact of ammonia on particle formation in the Asian Tropopause Aerosol Layer, npj Climate and Atmospheric Science, 7, 12–14, https://doi.org/10.1038/s41612-024-00758-3, 2024.

Xu, W., Croteau, P., Williams, L., Canagaratna, M., Onasch, T., Cross, E., Zhang, X., Robinson, W., Worsnop, D., and Jayne, J.: Laboratory characterization of an aerosol chemical speciation monitor with PM2.5 measurement capability, Aerosol Science and Technology, 51, 69–83, https://doi.org/10.1080/02786826.2016.1241859, 2017.

Yu, P., Toon, O. B., Neely, R. R., Martinsson, B. G., and Brenninkmeijer, C. A. M.: Composition and physical properties of the Asian Tropopause Aerosol Layer and the North American Tropospheric Aerosol Layer, Geophysical Research Letters, 42, 2540–2546, https://doi.org/10.1002/2015GL063181, 2015.

Yu, P., Rosenlof, K. H., Liu, S., Telg, H., Thornberry, T. D., Rollins, A. W., Portmann, R. W., Bai, Z., Ray, E. A., Duan, Y., Pan, L. L., Toon, O. B., Bian, J., and Gao, R.-S.: Efficient transport of tropospheric aerosol into the stratosphere via the Asian summer monsoon anticyclone, Proceedings of the National Academy of Sciences (PNAS), 114, 6972–6977, https://doi.org/10.1073/pnas.1701170114, 2017.

https://doi.org/10.5194/egusphere-2026-998
Preprint. Discussion started: 19 March 2026


Yu, P., Lian, S., Zhu, Y., Toon, O. B., Höpfner, M., and Borrmann, S.: Abundant nitrate and nitric acid aerosol in the upper troposphere and lower stratosphere, Geophysical Research Letters, 49, e2022GL100 258, https://doi.org/10.1029/2022GL100258, 2022.

Zahn, A. and Brenninkmeijer, C. A. M.: New Directions: A Chemical Tropopause Defined, Atmospheric Environment, 37, 439–440, https://doi.org/10.1016/S1352-2310(02)00901-9, 2003.

Zhang, Q., Wu, G., and Qian, Y.: The bimodality of the 100 hPa South Asia High and its relationship to the climate anomaly over East Asia in summer, Journal of the Meteorological Society of Japan, 80, 733–744, https://doi.org/10.2151/jmsj.80.733, 2002a.

Zhang, S., Solomon, S., Boone, C. D., and Taha, G.: Investigating the vertical extent of the 2023 summer Canadian wildfire impacts with satellite observations, Atmospheric Chemistry and Physics, 24, 11 727–11 736, https://doi.org/10.5194/acp-24-11727-2024, 2024.

Zhang, X., Smith, K. A., Worsnop, D. R., Jimenez, J., Jayne, J. T., and Kolb, C. E.: A Numerical Characterization of Particle Beam Collimation by an Aerodynamic Lens-Nozzle System: Part I. An Individual Lens or Nozzle, Aerosol Science and Technology, 36, 617–631, https://doi.org/10.1080/02786820252883856, 2002b.

Zhao, R., Zhang, Q., Xu, X., Wang, W., Zhao, W., Zhang, W., and Zhang, Y.: Effect of photooxidation on size distribution, light absorption, and molecular compositions of smoke particles from rice straw combustion, Environmental Pollution, 311, 119 950, https://doi.org/10.1016/j.envpol.2022.119950, 2022.

Zhu, Y., Yu, P., Wang, X., Bardeen, C., Borrmann, S., Höpfner, M., Mahnke, C., Weigel, R., Krämer, M., Deshler, T., Bian, J., Bai, Z., Vernier, H., Portmann, R. W., Rosenlof, K. H., Kloss, C., Pan, L. L., Smith, W., Honomichl, S., Zhang, J., Stone, K. A., and Toon, O. B.: Evaluating the importance of nitrate-containing aerosols for the Asian Tropopause Aerosol Layer, Journal of Geophysical Research: Atmospheres, 129, e2024JD041 283, https://doi.org/10.1029/2024JD041283, 2024.